

Secrecy Capacity Analysis and Beamforming Optimization for MIMO-VLC Wiretap Channels

Sufang Yang, Longguang Li, *Member, IEEE*, Jintao Wang, *Senior Member, IEEE*, Ya Li, Liang Xia, Hongjun He, Qixing Wang, and Guangyi Liu, *Member, IEEE*

Abstract—This paper investigates a multiple-input multiple-output (MIMO) visible light communication (VLC) wiretap channel consisting of a transmitter, a legitimate receiver, and an eavesdropper. The optical input is subject to both peak and average-intensity constraints. By applying the generalized entropy-power inequality to truncated exponential inputs, we derive a novel closed-form expression for the achievable secrecy rate for general MIMO VLC configurations. To enhance transmission confidentiality, a fully-connected beamforming scheme is proposed, along with a low-complexity sub-connected alternative. Although the resulting beamforming design problems are non-convex, they are efficiently addressed by transforming them into a sequence of convex subproblems solvable via the successive convex approximation framework. Numerical results demonstrate that the proposed schemes achieve significant secrecy performance improvements compared with the benchmark scheme.

Index Terms—Secrecy capacity, visible light communication (VLC), physical-layer security, beamforming, multiple-input multiple-output (MIMO) channel.

I. INTRODUCTION

With the accelerated evolution of intelligent transportation systems, vehicular networks place increasingly stringent requirements on wireless communications for vehicle-to-vehicle, vehicle-to-infrastructure, and vehicle-to-everything links. In particular, emerging vehicular applications necessitate the simultaneous provision of high throughput, ultra-low latency, massive connectivity, and high reliability. Such requirements expose the inherent limitations of conventional radio-frequency (RF) communication systems. Specifically, the scarcity of available spectrum has led to severe congestion in RF-based vehicular networks. To address this challenge, alternative wireless communication technologies are urgently needed to complement existing RF frameworks. Visible light communication (VLC) has emerged as a promising solution by exploiting the abundant spectrum in the 400-800 THz range

[1–3]. In VLC systems, information is modulated onto visible light and transmitted using light-emitting diodes (LEDs), serving dual functions for illumination and communication. The modulated light propagates through the optical wireless channel and is detected by photodetectors (PDs) at the receiver.

Owing to the broadcast nature of wireless transmission, any receiving node within the coverage area is capable of intercepting the transmitted signal, which creates a significant security risk when potential eavesdroppers (illegal receivers) coexist with legitimate receivers – a scenario modeled as a wiretap channel. To mitigate such security risks, physical-layer security (PLS) has been proposed to enhance confidentiality for legitimate transmissions by degrading the eavesdropper’s channel. Although extensive studies have established PLS results for RF wiretap channels [4–8], they cannot be directly extended to the VLC wiretap channels due to their fundamentally different channel characteristics. The key difference stems from the fact that VLC adopts the intensity-modulation direct-detection scheme. Thus, the input of the LED in VLC channels is real and nonnegative, in sharp contrast to the complex-valued input in RF channels. Moreover, the input is subject to a peak-intensity constraint to ensure that the LED operates within its linear range [9–11], as well as an average intensity constraint imposed by illumination requirements or safety considerations [12, 13]. Motivated by these distinctive characteristics, a growing body of research has investigated the secrecy capacity of VLC wiretap channels under PLS, which is defined as the maximum achievable secrecy rate at which the transmitter can securely communicate with the legitimate receiver in the presence of an eavesdropper.

For the single-input single-output (SISO) VLC wiretap channels, existing studies have characterized the secrecy capacity under various optical input constraints [14–19]. Under a single peak-intensity constraint, achievable secrecy rate is derived by employing uniformly distributed input, which naturally yields a lower bound on the secrecy capacity [14]. This lower bound is shown to be tight at high signal-to-noise ratio (SNR) but loose at low SNR. To further tighten the secrecy capacity bounds, alternative input distributions have been investigated, including truncated Gaussian distribution [15], truncated generalized normal distribution [16], and truncated discrete generalized normal distribution [17]. Beyond the single peak-intensity constraint, the secrecy capacity analysis has also been extended to scenarios with an average-intensity constraint alone, as well as combined peak- and average-intensity constraints, for which corresponding upper and lower bounds on the secrecy capacity are derived [18, 19].

This work was supported in part by the National Natural Science Foundation of China under Grant No. 62101192, in part by Shanghai Sailing Program under Grant No. 21YF1411000, and in part by Tsinghua University-China Mobile Research Institute Joint Innovation Center. (*Corresponding author: Longguang Li.*)

Sufang Yang, Ya Li, Liang Xia, Hongjun He, Qixing Wang, and Guangyi Liu are with the Future Research Laboratory, China Mobile Research Institute, Beijing 100053, China (e-mail: yangsufang@chinamobile.com).

Longguang Li is with SJTU Paris Elite Institute of Technology, Shanghai Jiao Tong University, Shanghai 200240, China (e-mail: llg9012@sjtu.edu.cn).

Jintao Wang is with the Beijing National Research Center for Information Science and Technology (BNRist), Tsinghua University, Beijing 100084, China, also with the Department of Electronic Engineering, Tsinghua University, Beijing 100084, China, and also with the Research Institute, Tsinghua University in Shenzhen, Shenzhen 518057, China (e-mail: wangjintao@tsinghua.edu.cn).

For the multiple-input single-output (MISO) wiretap channels, existing research focuses on enhancing the achievable secrecy rate through many PLS techniques. Representative approaches include beamforming [14, 20], friendly jamming (or artificial noise) [21, 22], and space modulation (SM) [23, 24]. Under the peak-intensity constraint and perfect eavesdropper channel state information (CSI), a beamforming scheme is proposed to maximize the achievable secrecy rate [14]. To tackle the issue arising from imperfect eavesdropper CSI, a robust beamforming scheme is developed to maximize the worst-case achievable secrecy rate within the eavesdropping region [20]. Alongside beamforming, friendly jamming effectively degrades the eavesdropper performance. Some studies assume that each LED simultaneously transmits an information-bearing signal and a randomly generated jamming signal [21], whereas others introduce a separate jammer dedicated solely to transmitting the jamming signal [22]. Furthermore, an SM scheme is leveraged to improve performance for the legitimate receiver. Different LED activation strategies are investigated, where a subset of LEDs is activated at any given time to transmit the signal [23], whereas only a single LED is activated at a time [24]. Building upon these individual techniques, cooperative PLS schemes that jointly exploit the aforementioned techniques have also been explored to further enhance secrecy performance [25–29].

For the multiple-input multiple-output (MIMO) VLC wiretap channels, several studies have extended the MISO results to this scenario [30–33]. Nevertheless, these approaches still exhibit notable limitations. Specifically, the works in [30] and [31] neglect essential optical input constraints. In contrast, [32] considers both peak- and average-intensity constraints; however, it relies on inappropriate modeling assumptions by treating the average intensity (i.e., the first-order moment) as a second-order moment, which contradicts fundamental characteristics of VLC signals [11–13]. Furthermore, although the work in [33] correctly incorporates the peak-intensity constraint to derive the achievable secrecy rate¹, its formulation is computationally intensive, involves multiple undetermined design parameters, and is restricted to this single type of input constraint.

To the best of our knowledge, the MIMO-VLC wiretap channels under both peak-intensity and average-intensity constraints have not yet been systematically investigated. Consequently, a concise and tractable closed-form expression for the achievable secrecy rate is still lacking, which is of fundamental importance for both theoretical analysis and practical system design. The main contributions are summarized as follows.

- By applying the generalized entropy-power inequality (GEPI) to the truncated exponential input, we derive closed-form achievable secrecy rates for the MIMO-VLC wiretap channels. Different quantitative relationships be-

¹In [33], the authors consider that the input \mathbf{X} is subject to both peak- and average-intensity constraints such that $\Pr\{|X_i| \leq A\} = 1$ and $\mathbf{E}\{X_i\} = 0$, $\forall i \in \{1, \dots, n_T\}$. However, it can be shown that in (4), $\alpha_i = \frac{1}{2}$ for all i , indicating that the average-intensity constraint is inactive [11, Lem. 2], [34, Lem. 1] [35, Prop. 1]. Consequently, the analysis in [33] effectively corresponds to the scenario in which a single peak-intensity constraint is imposed on the input.

tween the number of transmit and receive apertures are discussed; see Theorem 2.

- Two novel beamforming schemes, termed fully-connected and sub-connected beamforming schemes, are proposed to enhance the PLS of the MIMO-VLC wiretap channel. The optimal beamformer for each scheme is formulated by an optimization problem maximizing the derived achievable secrecy rate. The conventional zero-forcing (ZF) beamforming scheme is also analyzed as a benchmark; see Sec. IV.
- To reduce the complexity of finding the optimal beamformer, we use the Taylor approximation to transform the original non-convex beamforming optimization problem into a sequence of convex subproblems. Novel algorithms are then proposed to iteratively solve these subproblems and find the optimal beamformer that maximizes the achievable secrecy rate; see Algorithms 1, 2, and 3.

The remaining part of this paper is organized as follows. Sec. II introduces the MIMO-VLC wiretap channel model. Sec. III formulates the achievable secrecy rates. Secs. IV and V propose beamforming schemes and the corresponding algorithms. Simulation results are provided in Sec. VI. We conclude this paper in Sec. VII. A few proofs are given in the Appendix.

Notation: Scalars are denoted by non-bolded letters, e.g., X denotes a random scalar and x its realization. Vectors are denoted by boldfaced letters, e.g., \mathbf{X} denotes a random vector and \mathbf{x} its realization. All the matrices in this paper are deterministic and typeset in a blackboard-bold font, e.g., \mathbb{H} . Mutual information is denoted by $I(\cdot; \cdot)$, entropy by $h(\cdot)$, expectation by $\mathbf{E}\{\cdot\}$, and covariance by $\text{Cov}\{\cdot\}$. The absolute determinant of matrices is denoted by $|\cdot|$, the transposition by $(\cdot)^T$, the trace by $\text{tr}\{\cdot\}$, and the vectorization by $\text{vec}(\cdot)$. 1-norm of matrices is denoted by $\|\cdot\|_1$, and the Frobenius norm by $\|\cdot\|_F$. The set of real numbers is denoted by \mathcal{R} , nonnegative real numbers by \mathcal{R}_+ , and n -dimensional positive semi-definite matrices by \mathcal{S}_+^n . \mathbb{I}_m denotes an $(m \times m)$ -dimensional identity matrix, and \mathbf{e}_j denotes a unit vector with the j -th entry equal to 1. $\mathbf{0}_m$ and $\mathbf{1}_m$ denote column vectors of length m with all entries equal to 0 and 1, respectively. $\mathbf{0}_{m \times n}$ and $\mathbf{1}_{m \times n}$ denote $(m \times n)$ -dimensional matrices with all entries equal to 0 and 1, respectively.

II. CHANNEL MODEL

Consider an MIMO-VLC wiretap channel consisting of a transmitter Alice, a legitimate receiver Bob, and an eavesdropper Eve. Alice aims to communicate messages to Bob while preventing eavesdropping by Eve. We use subscripts $(\cdot)_B$ and $(\cdot)_E$ to distinguish parameters associated with Bob and Eve, respectively. Assume Alice has n_T LEDs, while Bob and Eve have n_B and n_E PDs, respectively. A fixed direct current bias, $I_{DC} \in \mathcal{R}_+$, is introduced to ensure that the LED's input is nonnegative [36]. As it can be effectively removed by a capacitor at the receiver, the channel outputs observed at Bob and Eve are characterized by

$$\mathbf{Y}_B = \xi \mathbb{H}_B \mathbf{X} + \mathbf{Z}_B, \quad (1a)$$

$$\mathbf{Y}_E = \xi \mathbb{H}_E \mathbf{X} + \mathbf{Z}_E, \quad (1b)$$

with the photoelectric coefficient $\xi \in \mathcal{R}_+$, the channel matrices $\mathbb{H}_B \in \mathcal{R}_+^{n_B \times n_T}$ and $\mathbb{H}_E \in \mathcal{R}_+^{n_E \times n_T}$, the data input $\mathbf{X} \in \mathcal{R}^{n_T}$, the outputs $\mathbf{Y}_B \in \mathcal{R}^{n_B}$ and $\mathbf{Y}_E \in \mathcal{R}^{n_E}$, and the noises $\mathbf{Z}_B \in \mathcal{R}^{n_B}$ and $\mathbf{Z}_E \in \mathcal{R}^{n_E}$, following Gaussian distributions $\mathcal{N}(\mathbf{0}_{n_B}, \sigma_B^2 \mathbb{I}_{n_B})$ and $\mathcal{N}(\mathbf{0}_{n_E}, \sigma_E^2 \mathbb{I}_{n_E})$, respectively. Without loss of generality, we assume $\xi = 1$ and $\sigma_B^2 = \sigma_E^2 = 1$. Throughout the paper, we assume that Alice knows Eve's CSI [25]. We also assume that \mathbb{H}_B and \mathbb{H}_E are of full ranks, consistent with the setup in existing works [35, 37, 38]².

Considering the limited dynamic range and illumination requirement of LEDs [9–13], the input \mathbf{X} is subject to the following constraints:

- Peak-intensity constraint:

$$\Pr\{|X_i| \leq A\} = 1, \quad \forall i \in \{1, \dots, n_T\}, \quad (2)$$

- Average-intensity constraint:

$$\mathbb{E}\{X_i\} = E_i, \quad \forall i \in \{1, \dots, n_T\}, \quad (3)$$

where X_i denotes the i -th entry of \mathbf{X} . For convenience, we define the vector $\boldsymbol{\alpha} = (\alpha_1, \dots, \alpha_{n_T})^\top$ with

$$\alpha_i = \frac{E_i + A}{2A}, \quad \forall i \in \{1, \dots, n_T\}. \quad (4)$$

It is direct to see $\alpha_i \in (0, 1)$ [11]. We also define the vector $\boldsymbol{\beta} = (\beta_1, \dots, \beta_{n_T})^\top$ with $\boldsymbol{\beta} = \boldsymbol{\alpha} - \frac{1}{2}\mathbf{1}_{n_T}$.

In this wiretap channel, the secrecy capacity C_s , denoting the maximum achievable secrecy rate between Alice and Bob in the presence of Eve, is characterized by the following lemma:

Lemma 1 ([39, Cor. 2], [40, Thm. 22.1]): The secrecy capacity for the wiretap channel in (1) is given by

$$C_s = \max_{\mathbf{U}, \mathbf{X}} \{I(\mathbf{U}; \mathbf{Y}_B) - I(\mathbf{U}; \mathbf{Y}_E)\}, \quad (5)$$

where \mathbf{U} is an auxiliary variable and $\mathbf{U} \rightarrow \mathbf{X} \rightarrow (\mathbf{Y}_B, \mathbf{Y}_E)$ form a Markov chain. ■

III. ACHIEVABLE SECRECY RATE CHARACTERIZATION

This section presents the achievable secrecy rate of the MIMO-VLC wiretap channel. By setting $\mathbf{U} = \mathbf{X}$, the secrecy capacity can be lower-bounded as

$$C_s \geq \max_{\mathbf{p}, \mathbf{x}} \{I(\mathbf{X}; \mathbf{Y}_B) - I(\mathbf{X}; \mathbf{Y}_E)\}. \quad (6)$$

To satisfy the constraints in (2) and (3), we employ a truncated exponential distribution \mathbf{X}_{te} , which performs well in a scalar point-to-point VLC channel and achieves channel capacity at high SNR [11, 35, 37]. Its distribution is given by

$$p_{\mathbf{X}_{te}}(\mathbf{x}) = \prod_{i=1}^{n_T} \frac{1}{2A} \cdot \frac{\mu_i}{1 - e^{-\mu_i}} e^{-\frac{\mu_i(x_i + A)}{2A}}, \quad x_i \in [-A, A], \quad (7)$$

where x_i denotes the i -th entry of \mathbf{x} , and μ_i is the unique solution to

$$\frac{1}{\mu_i} - \frac{e^{-\mu_i}}{1 - e^{-\mu_i}} = \alpha_i, \quad i \in \{1, \dots, n_T\}. \quad (8)$$

²As demonstrated in [35, Sec. III-C] and [37, Appendix A], any channel model can be reduced via singular value decomposition (SVD) to an equivalent channel model with a full-rank channel matrix. This simplification streamlines the secrecy capacity analysis without loss of generality.

Substituting (7) into (6), the secrecy capacity in (6) can be further lower-bounded as

$$C_s \geq I(\mathbf{X}_{te}; \mathbf{Y}_B) - I(\mathbf{X}_{te}; \mathbf{Y}_E). \quad (9)$$

It is worth noting that (9) can be efficiently analyzed based on quantitative relationships between the number of transmit and receive apertures [35, 37, 38]. We classify the secrecy capacity into two primary cases in this paper³:

- Case I: the number of LEDs is larger than or equal to the number of PDs, i.e., $n_T \geq n_B$ and $n_T \geq n_E$;
- Case II: the number of LEDs is less than the number of PDs, i.e., $n_T < n_B$ and $n_T < n_E$.

We summarize the main results in the following theorem.

Theorem 2: For Case I, an achievable secrecy rate is given by:

$$\begin{aligned} R_s^I(\mathbb{H}_B, \mathbb{H}_E) &= \frac{n_B}{2} \log \left(1 + |\mathbb{H}_B \cdot \text{diag}(\mathbf{p}) \cdot \mathbb{H}_B^\top|^{\frac{1}{n_B}} \right) \\ &\quad - \frac{1}{2} \log |\mathbb{H}_E \cdot \text{diag}(\mathbf{v}) \cdot \mathbb{H}_E^\top + \mathbb{I}_{n_E}|, \end{aligned} \quad (10)$$

for Case II:

$$\begin{aligned} R_s^{II}(\mathbb{H}_B, \mathbb{H}_E) &= \frac{n_T}{2} \log \left(1 + |\text{diag}(\mathbf{p})|^{\frac{1}{n_T}} \cdot |\mathbb{H}_B^\top \mathbb{H}_B|^{\frac{1}{n_T}} \right) \\ &\quad - \frac{1}{2} \log |\text{diag}(\mathbf{v}) \cdot \mathbb{H}_E^\top \mathbb{H}_E + \mathbb{I}_{n_T}|, \end{aligned} \quad (11)$$

where vectors $\mathbf{p} = (p_1, \dots, p_{n_T})^\top$ and $\mathbf{v} = (v_1, \dots, v_{n_T})^\top$, with $\forall i \in \{1, \dots, n_T\}$,

$$p_i = 2A^2 \frac{e^{2\alpha_i \mu_i}}{\pi e} \left(\frac{1 - e^{-\mu_i}}{\mu_i} \right)^2, \quad (12)$$

$$v_i = A^2 \left(\frac{8}{\mu_i^2} - \frac{4e^{-\mu_i} + 4}{\mu_i(1 - e^{-\mu_i})} - 4\alpha_i^2 + 4\alpha_i \right). \quad (13)$$

The proofs of (10) and (11) are given in Secs. III-A and III-B, respectively. ■

A. Proof of Achievable Secrecy Rate for Case I

We first derive a lower bound on $I(\mathbf{X}_{te}; \mathbf{Y}_B)$ and then an upper bound on $I(\mathbf{X}_{te}; \mathbf{Y}_E)$. The lower bound derivation begins with

$$I(\mathbf{X}_{te}; \mathbf{Y}_B) = h(\mathbb{H}_B \mathbf{X}_{te} + \mathbf{Z}_B) - h(\mathbf{Z}_B) \quad (14)$$

$$\geq \frac{n_B}{2} \log \left(1 + \frac{e^{\frac{2}{n_B} h(\mathbb{H}_B \mathbf{X}_{te})}}{e^{\frac{2}{n_B} h(\mathbf{Z}_B)}} \right) \quad (15)$$

$$\geq \frac{n_B}{2} \log \left(1 + |\mathbb{H}_B \cdot \text{diag}(\mathbf{p}) \cdot \mathbb{H}_B^\top|^{\frac{1}{n_B}} \right), \quad (16)$$

where (15) holds by the entropy power inequality (EPI) and (16) by the GEPI [41]:

$$h(\mathbb{H}_B \mathbf{X}_{te}) \geq \frac{n_B}{2} \log \left(2\pi e |\mathbb{H}_B \cdot \text{diag}(\mathbf{p}) \cdot \mathbb{H}_B^\top|^{\frac{1}{n_B}} \right), \quad (17)$$

where $\mathbf{p} = \left(\frac{e^{2h(X_{te,1})}}{2\pi e}, \dots, \frac{e^{2h(X_{te,n_T})}}{2\pi e} \right)^\top$ with $X_{te,i}$ denoting the i -th entry of \mathbf{X}_{te} , $i \in \{1, \dots, n_T\}$. Then, we compute the entropy $h(X_{te,i})$ using (7), and obtain the vector \mathbf{p} in (12).

³The analysis for (a) $n_T \geq n_B$ and $n_T < n_E$, (b) $n_T < n_B$ and $n_T \geq n_E$, follow similar procedures as in Secs. III-A and III-B, which are omitted here.

Next, an upper bound on $I(\mathbf{X}_{te}; \mathbf{Y}_E)$ can be obtained by

$$I(\mathbf{X}_{te}; \mathbf{Y}_E) = h(\mathbb{H}_E \mathbf{X}_{te} + \mathbf{Z}_E) - h(\mathbf{Z}_E) \quad (18)$$

$$\leq \frac{n_E}{2} \log(2\pi e) + \frac{1}{2} \log |\text{Cov}\{\mathbb{H}_E \mathbf{X}_{te} + \mathbf{Z}_E\}| - h(\mathbf{Z}_E) \quad (19)$$

$$= \frac{1}{2} \log |\mathbb{H}_E \cdot \text{diag}(\mathbf{v}) \cdot \mathbb{H}_E^T + \mathbb{I}_{n_E}|, \quad (20)$$

where (19) follows from the principle of maximum entropy, i.e., the entropy of $(\mathbb{H}_E \mathbf{X}_{te} + \mathbf{Z}_E)$ can be upper-bounded by the entropy of a Gaussian random vector with the same covariance matrix. With (7), we can obtain the vector \mathbf{v} in (13).

Substituting (16) and (20) into (9), we obtain (10).

B. Proof of Achievable Secrecy Rate for Case II

To derive a lower bound on $I(\mathbf{X}_{te}; \mathbf{Y}_B)$, we decompose \mathbb{H}_B via SVD as $\mathbb{H}_B = \mathbb{U}_B \mathbb{S}_B \mathbb{V}_B$. Here, the orthogonal matrices $\mathbb{U}_B \in \mathcal{R}^{n_B \times n_B}$, $\mathbb{V}_B \in \mathcal{R}^{n_T \times n_T}$, and the rectangular diagonal matrix $\mathbb{S}_B \in \mathcal{R}^{n_B \times n_T}$, with $\mathbb{S}_B^{n_T}$ being the first n_T rows. We bound $I(\mathbf{X}_{te}; \mathbf{Y}_B)$ by

$$I(\mathbf{X}_{te}; \mathbf{Y}_B) = I(\mathbf{X}_{te}; \mathbb{S}_B \mathbb{V}_B \mathbf{X}_{te} + \mathbf{Z}'_B) \quad (21)$$

$$= I(\mathbf{X}_{te}; \mathbb{S}_B^{n_T} \mathbb{V}_B \mathbf{X}_{te} + \mathbf{Z}''_B) \quad (22)$$

$$= I(\mathbf{X}_{te}; \mathbf{X}_{te} + \mathbb{V}_B^T (\mathbb{S}_B^{n_T})^{-1} \mathbf{Z}''_B) \quad (23)$$

$$= h(\mathbf{X}_{te} + \mathbb{V}_B^T (\mathbb{S}_B^{n_T})^{-1} \mathbf{Z}''_B) - h(\mathbb{V}_B^T (\mathbb{S}_B^{n_T})^{-1} \mathbf{Z}''_B) \quad (24)$$

$$\geq \frac{n_T}{2} \log \left(1 + \frac{e^{\frac{2}{n_T} \sum_{i=1}^{n_T} h(X_{te,i})}}{e^{\frac{2}{n_T} h(\mathbb{V}_B^T (\mathbb{S}_B^{n_T})^{-1} \mathbf{Z}''_B)}} \right), \quad (25)$$

where $\mathbf{Z}'_B = \mathbb{U}_B^T \mathbf{Z}_B$, \mathbf{Z}''_B represents the first n_T rows of \mathbf{Z}'_B , and (25) holds by the EPI. Note that $\mathbb{V}_B^T (\mathbb{S}_B^{n_T})^{-1} \mathbf{Z}''_B$ is an n_T -dimensional Gaussian random vector since $\mathbf{Z}''_B \sim \mathcal{N}(\mathbf{0}_{n_T}, \mathbb{I}_{n_T})$. Its covariance matrix is given by

$$\text{Cov}\{\mathbb{V}_B^T (\mathbb{S}_B^{n_T})^{-1} \mathbf{Z}''_B\} = \mathbb{V}_B^T (\mathbb{S}_B^{n_T})^{-1} (\mathbb{S}_B^{n_T})^{-T} \mathbb{V}_B \quad (26)$$

$$= \left(\mathbb{V}_B^T (\mathbb{S}_B^{n_T})^T (\mathbb{S}_B^{n_T}) \mathbb{V}_B \right)^{-1} \quad (27)$$

$$= (\mathbb{V}_B^T \mathbb{S}_B^T \mathbb{S}_B \mathbb{V}_B)^{-1} \quad (28)$$

$$= (\mathbb{H}_B^T \mathbb{H}_B)^{-1}. \quad (29)$$

Therefore,

$$h(\mathbb{V}_B^T (\mathbb{S}_B^{n_T})^{-1} \mathbf{Z}''_B) = \frac{n_T}{2} \log(2\pi e) + \frac{1}{2} \log |\text{Cov}\{\mathbb{V}_B^T (\mathbb{S}_B^{n_T})^{-1} \mathbf{Z}''_B\}| \quad (30)$$

$$= \frac{n_T}{2} \log(2\pi e) - \frac{1}{2} \log |\mathbb{H}_B^T \mathbb{H}_B|. \quad (31)$$

Substituting (31) into (25), we have

$$I(\mathbf{X}_{te}; \mathbf{Y}_B) \geq \frac{n_T}{2} \log \left\{ 1 + |\text{diag}(\mathbf{p})|^{\frac{1}{n_T}} \cdot |\mathbb{H}_B^T \mathbb{H}_B|^{\frac{1}{n_T}} \right\}. \quad (32)$$

To derive an upper bound on $I(\mathbf{X}_{te}; \mathbf{Y}_E)$, we also decompose \mathbb{H}_E via SVD as $\mathbb{H}_E = \mathbb{U}_E \mathbb{S}_E \mathbb{V}_E$, where the orthogonal matrices $\mathbb{U}_E \in \mathcal{R}^{n_E \times n_E}$, $\mathbb{V}_E \in \mathcal{R}^{n_T \times n_T}$, and the rectangular diagonal

matrix $\mathbb{S}_E \in \mathcal{R}^{n_E \times n_T}$, with $\mathbb{S}_E^{n_T}$ being the first n_T rows. Similarly, we derive

$$I(\mathbf{X}_{te}; \mathbf{Y}_E) = h(\mathbf{X}_{te} + \mathbb{V}_E^T (\mathbb{S}_E^{n_T})^{-1} \mathbf{Z}''_E) - h(\mathbb{V}_E^T (\mathbb{S}_E^{n_T})^{-1} \mathbf{Z}''_E) \quad (33)$$

$$= h(\mathbf{X}_{te} + \mathbb{V}_E^T (\mathbb{S}_E^{n_T})^{-1} \mathbf{Z}''_E) - \frac{n_T}{2} \log(2\pi e) + \frac{1}{2} \log |\mathbb{H}_E^T \mathbb{H}_E| \quad (34)$$

$$\leq \frac{1}{2} \log |\text{Cov}\{\mathbf{X}_{te} + \mathbb{V}_E^T (\mathbb{S}_E^{n_T})^{-1} \mathbf{Z}''_E\}| + \frac{1}{2} \log |\mathbb{H}_E^T \mathbb{H}_E| \quad (35)$$

$$= \frac{1}{2} \log |\text{diag}(\mathbf{v}) \cdot \mathbb{H}_E^T \mathbb{H}_E + \mathbb{I}_{n_T}|, \quad (36)$$

where \mathbf{Z}''_E denotes the first n_T rows of $\mathbb{U}_E^T \mathbf{Z}_E$, (34) follows because $\mathbb{V}_E^T (\mathbb{S}_E^{n_T})^{-1} \mathbf{Z}''_E \sim \mathcal{N}(\mathbf{0}_{n_T}, (\mathbb{H}_E^T \mathbb{H}_E)^{-1})$, and (35) holds by the principle of maximum entropy.

Substituting (32) and (36) into (9) yields (11).

IV. MIMO-VLC WIRETAP CHANNEL BEAMFORMING DESIGN

This section proposes beamforming schemes to enhance the secrecy performance of the MIMO-VLC wiretap channels. We first analyze Case I, and then proceed to Case II.

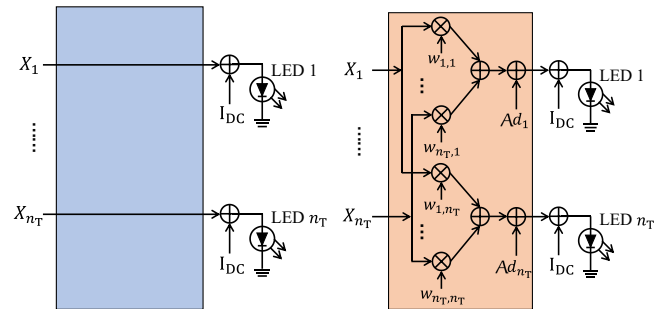
A. Beamforming Design for Case I

1) *Fully-connected Beamforming Design*: A linear transformation is applied to the input signals across different LEDs such that

$$\mathbf{Y}_B = \mathbb{H}_B (\mathbb{W}^T \mathbf{X} + \text{Ad}) + \mathbf{Z}_B, \quad (37a)$$

$$\mathbf{Y}_E = \mathbb{H}_E (\mathbb{W}^T \mathbf{X} + \text{Ad}) + \mathbf{Z}_E, \quad (37b)$$

where $\mathbb{W} \in \mathcal{R}^{n_T \times n_T}$ is the beamforming matrix and $\mathbf{d} \in \mathcal{R}^{n_T}$ is a bias vector. Note that (1) represents a special case of (37) when $\mathbb{W} = \mathbb{I}_{n_T}$ and $\mathbf{d} = \mathbf{0}_{n_T}$. In (37), each input X_j is fed to all LEDs through the beamformer \mathbb{W} , while in (1), X_j is directly connected solely to the j -th LED, $j \in \{1, \dots, n_T\}$. For clarity, we refer to (37) as the fully-connected beamforming scheme and (1) as the direct-connected beamforming scheme, and their comparison is illustrated in Fig. 1.



(a) Direct-connected beamformer. (b) Fully-connected beamformer.

Fig. 1: Architectures of two beamforming schemes: (a) Direct-connected beamformer: the j -th LED is only connected to the j -th input X_j ; (b) Fully-connected beamformer: each LED is connected to all inputs X_j s, $j \in \{1, \dots, n_T\}$.

Denote $\mathbb{W} = (\mathbf{w}_1, \dots, \mathbf{w}_{n_T})$. To satisfy the peak-intensity constraint for LEDs, it suffices that $\forall j \in \{1, \dots, n_T\}$,

$$\|\mathbf{w}_j\|_1 + d_j \leq 1, \quad (38a)$$

$$-\|\mathbf{w}_j\|_1 + d_j \geq -1. \quad (38b)$$

Additionally, satisfying the average-intensity constraint requires that $\forall j \in \{1, \dots, n_T\}$,

$$\mathbf{w}_j^T \boldsymbol{\beta} + \frac{1}{2} d_j = \beta_j. \quad (39)$$

We have $\|\mathbf{w}_j\|_1 \leq 1$ from (38). Combining this with (39), a feasible d_j exists if $|d_j| \leq 1 - \|\mathbf{w}_j\|_1$. Hence, both constraints are satisfied if and only if $\forall j \in \{1, \dots, n_T\}$,

$$\|\mathbf{w}_j\|_1 \leq 1, \quad (40a)$$

$$|\mathbf{w}_j^T \boldsymbol{\beta} - \beta_j| \leq \frac{1}{2} - \frac{1}{2} \|\mathbf{w}_j\|_1. \quad (40b)$$

Note that the equivalent channel matrices of Bob and Eve become $\mathbb{H}_B \mathbb{W}^T$ and $\mathbb{H}_E \mathbb{W}^T$, respectively⁴. Substituting them into (10), the optimal fully-connected beamformer \mathbb{W}_{FC}^* maximizing the achievable secrecy rate can be obtained by:

$$\mathcal{P}_1 : \mathbb{W}_{\text{FC}}^* = \underset{\mathbb{W}}{\operatorname{argmax}} \{R_s^I(\mathbb{H}_B \mathbb{W}^T, \mathbb{H}_E \mathbb{W}^T)\} \quad (41)$$

$$\text{s.t.} \begin{cases} \|\mathbf{w}_j\|_1 \leq 1, \forall j, \\ |\mathbf{w}_j^T \boldsymbol{\beta} - \beta_j| \leq \frac{1}{2} - \frac{1}{2} \|\mathbf{w}_j\|_1, \forall j. \end{cases} \quad (42)$$

Next, we analyze the fully-connected ZF beamforming scheme for the MIMO-VLC wiretap channel. This scheme restricts the beamformer to lie within Eve's nullspace, i.e.,

$$\mathbb{H}_E \mathbb{W}^T = \mathbf{0}_{n_E \times n_T}. \quad (43)$$

Consequently, the optimal fully-connected ZF beamformer \mathbb{W}_{ZF}^* is obtained by:

$$\mathcal{P}_2 : \mathbb{W}_{\text{ZF}}^* = \underset{\mathbb{W}}{\operatorname{argmax}} \{R_s^I(\mathbb{H}_B \mathbb{W}^T, \mathbb{H}_E \mathbb{W}^T)\} \quad (44)$$

$$\text{s.t.} \begin{cases} \|\mathbf{w}_j\|_1 \leq 1, \forall j, \\ |\mathbf{w}_j^T \boldsymbol{\beta} - \beta_j| \leq \frac{1}{2} - \frac{1}{2} \|\mathbf{w}_j\|_1, \forall j, \\ \mathbb{H}_E \mathbb{W}^T = \mathbf{0}_{n_E \times n_T}. \end{cases} \quad (45)$$

2) *Sub-connected Beamforming Design*: This section proposes a low-complexity beamforming scheme as an alternative to the fully-connected architecture. Denote \mathcal{I} as a rank(\mathbb{H}_B)-size subset of $\{1, 2, \dots, n_T\}$ and it is chosen such that $|\mathbb{H}_{B,\mathcal{I}}| \neq 0$, where $\mathbb{H}_{B,\mathcal{I}}$ is the submatrix of \mathbb{H}_B with columns indexed by \mathcal{I} . For convenience, \mathcal{I}_{all} denotes the set of all \mathcal{I} s satisfying $|\mathbb{H}_{B,\mathcal{I}}| \neq 0$.⁵ Using \mathcal{I} , the channel outputs in (1) can be reformulated as

$$\mathbf{Y}_B = \mathbb{H}_{B,\mathcal{I}} \mathbf{X}_{\mathcal{I}} + \mathbb{H}_{B,\mathcal{I}^c} \mathbf{X}_{\mathcal{I}^c} + \mathbf{Z}_B, \quad (46a)$$

$$\mathbf{Y}_E = \mathbb{H}_{E,\mathcal{I}} \mathbf{X}_{\mathcal{I}} + \mathbb{H}_{E,\mathcal{I}^c} \mathbf{X}_{\mathcal{I}^c} + \mathbf{Z}_E, \quad (46b)$$

where \mathcal{I}^c denotes the complement of \mathcal{I} , i.e., $\mathcal{I}^c = \{1, 2, \dots, n_T\} \setminus \mathcal{I}$; $\mathbf{X}_{\mathcal{I}}$ and $\mathbf{X}_{\mathcal{I}^c}$ are the subvectors of \mathbf{X} with entries indexed by \mathcal{I} and \mathcal{I}^c , respectively⁶; $\mathbb{H}_{B,\mathcal{I}^c}$, $\mathbb{H}_{E,\mathcal{I}}$, and

⁴It should be noted that constants $A\mathbb{H}_B \mathbf{d}$ and $A\mathbb{H}_E \mathbf{d}$ only have an effect on the input constraint without influencing the value of achievable secrecy rate.

⁵For example, if \mathbb{H}_B is a (2×3) -dimensional matrix with $\mathbb{H}_B = (\mathbf{h}_1, \mathbf{h}_2, \mathbf{h}_3)$ and $\operatorname{rank}(\mathbb{H}_B) = 2$. Then \mathcal{I} may be $\{1, 2\}$, $\{1, 3\}$, $\{2, 3\}$, the corresponding $\mathbb{H}_{B,\mathcal{I}}$ is $(\mathbf{h}_1, \mathbf{h}_2)$, $(\mathbf{h}_1, \mathbf{h}_3)$, $(\mathbf{h}_2, \mathbf{h}_3)$, and \mathcal{I}_{all} is $\{\{1, 2\}, \{1, 3\}, \{2, 3\}\}$.

⁶For example, if $\mathbf{X} = (8, 6, 7)^T$, $\mathcal{I} = \{1, 2\}$, and $\mathcal{I}^c = \{3\}$, then $\mathbf{X}_{\mathcal{I}} = (8, 6)^T$, and $\mathbf{X}_{\mathcal{I}^c} = 7$.

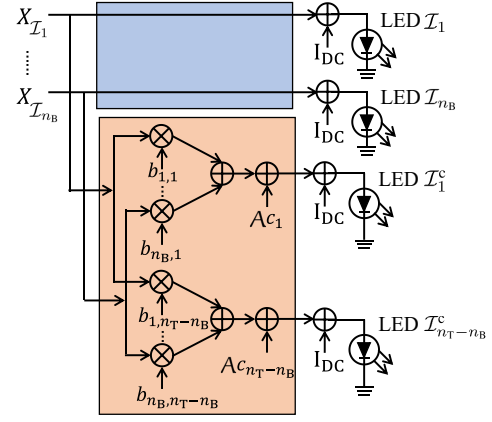


Fig. 2: Architecture of sub-connected beamforming scheme: the \mathcal{I}_j -th LED is only connected to the \mathcal{I}_j -th input $X_{\mathcal{I}_j}$, while the \mathcal{I}_k^c -th LED is connected to all inputs $X_{\mathcal{I}_j}$ s, where $\mathcal{I}_j \in \mathcal{I}$, $j \in \{1, \dots, n_B\}$, $\mathcal{I}_k^c \in \mathcal{I}^c$, and $k \in \{1, \dots, n_T - n_B\}$.

$\mathbb{H}_{E,\mathcal{I}^c}$ are the submatrices of \mathbb{H}_B , \mathbb{H}_E and \mathbb{H}_E with columns indexed by \mathcal{I}^c , \mathcal{I} , and \mathcal{I}^c , respectively.

Let \mathbb{B} be an $n_B \times (n_T - n_B)$ -dimensional matrix with $\mathbb{B} = (\mathbf{b}_1, \dots, \mathbf{b}_{n_T - n_B})$, and \mathbf{c} be an $(n_T - n_B)$ -dimensional vector with $\mathbf{c} = (c_1, \dots, c_{n_T - n_B})^T$. The sub-connected beamforming scheme designs the subvector $\mathbf{X}_{\mathcal{I}^c}$ to be a linear combination of the subvector $\mathbf{X}_{\mathcal{I}}$ such that

$$\mathbf{X}_{\mathcal{I}^c} = \mathbb{B}^T \mathbf{X}_{\mathcal{I}} + A\mathbf{c}. \quad (47)$$

Substituting it into (46), we obtain

$$\mathbf{Y}_B = (\mathbb{H}_{B,\mathcal{I}} + \mathbb{H}_{B,\mathcal{I}^c} \mathbb{B}^T) \mathbf{X}_{\mathcal{I}} + \mathbf{Z}_B + A\mathbb{H}_{B,\mathcal{I}^c} \mathbf{c}, \quad (48a)$$

$$\mathbf{Y}_E = (\mathbb{H}_{E,\mathcal{I}} + \mathbb{H}_{E,\mathcal{I}^c} \mathbb{B}^T) \mathbf{X}_{\mathcal{I}} + \mathbf{Z}_E + A\mathbb{H}_{E,\mathcal{I}^c} \mathbf{c}. \quad (48b)$$

Fig. 2 illustrates this sub-connected beamforming architecture. Note that (48) is a special case of the fully-connected beamforming scheme (37). For example, when $\mathcal{I} = \{1, \dots, n_B\}$ and $|\mathbb{H}_{B,\mathcal{I}}| \neq 0$, define

$$\mathbb{W} = \begin{pmatrix} \mathbb{I}_{n_B} & \mathbb{B} \\ \mathbf{0}_{(n_T - n_B) \times n_B} & \mathbf{0}_{(n_T - n_B) \times (n_T - n_B)} \end{pmatrix}, \quad (49)$$

$$\mathbf{d} = \begin{pmatrix} \mathbf{0}_{n_B} \\ \mathbf{c} \end{pmatrix}. \quad (50)$$

Substituting them into (37) yields (48).

Under the sub-connected beamforming architecture, the peak- and average-intensity constraints are satisfied if $\forall j \in \{1, \dots, n_T - n_B\}$,

$$-\|\mathbf{b}_j\|_1 + c_j \geq -1, \quad (51a)$$

$$\|\mathbf{b}_j\|_1 + c_j \leq 1, \quad (51b)$$

$$\mathbf{b}_j^T \boldsymbol{\beta}_{\mathcal{I}} + \frac{1}{2} c_j = \beta_{\mathcal{I}^c_j}, \quad (51c)$$

where $\boldsymbol{\beta}_{\mathcal{I}}$ and $\boldsymbol{\beta}_{\mathcal{I}^c}$ denote the subvectors of $\boldsymbol{\beta}$ with entries indexed by \mathcal{I} and \mathcal{I}^c , respectively, and $\beta_{\mathcal{I}^c_j}$ is the j -th entry of $\boldsymbol{\beta}_{\mathcal{I}^c}$. Analogous to (40), the inequalities in (51) are equivalent to

$$\|\mathbf{b}_j\|_1 \leq 1, \quad (52)$$

$$|\mathbf{b}_j^T \boldsymbol{\beta}_{\mathcal{I}} - \beta_{\mathcal{I}^c_j}| \leq \frac{1}{2} - \frac{1}{2} \|\mathbf{b}_j\|_1. \quad (53)$$

Note that in (48), the equivalent channel matrices of Bob and Eve are $(\mathbb{H}_{\mathbb{B},\mathcal{I}} + \mathbb{H}_{\mathbb{B},\mathcal{I}^c}\mathbb{B}^\top)$ and $(\mathbb{H}_{\mathbb{E},\mathcal{I}} + \mathbb{H}_{\mathbb{E},\mathcal{I}^c}\mathbb{B}^\top)$, respectively. Substituting them into (10), the optimal sub-connected beamformer \mathbb{B}_{SC}^* maximizing the achievable secrecy rate is found by:

$$\mathcal{P}_3 : (\mathbb{B}_{\text{SC}}^*, \mathcal{I}_{\text{SC}}^*) = \underset{\mathbb{B}, \mathcal{I}}{\operatorname{argmax}} \{ \mathbf{R}_s^{\text{I}}(\mathbb{H}_{\mathbb{B},\mathcal{I}} + \mathbb{H}_{\mathbb{B},\mathcal{I}^c}\mathbb{B}^\top, \mathbb{H}_{\mathbb{E},\mathcal{I}} + \mathbb{H}_{\mathbb{E},\mathcal{I}^c}\mathbb{B}^\top) \} \quad (54)$$

$$\text{s.t.} \begin{cases} \|\mathbf{b}_j\|_1 \leq 1, \forall j, \\ |\mathbf{b}_j^\top \boldsymbol{\beta}_{\mathcal{I}} - \beta_{\mathcal{I}^c_j}| \leq \frac{1}{2} - \frac{1}{2}\|\mathbf{b}_j\|_1, \forall j. \end{cases} \quad (55)$$

Next, we analyze the sub-connected ZF beamforming scheme for the MIMO-VLC wiretap channel. This is achieved by imposing the constraint:

$$\mathbb{H}_{\mathbb{E},\mathcal{I}^c}\mathbb{B}^\top = -\mathbb{H}_{\mathbb{E},\mathcal{I}}. \quad (56)$$

Thus, the optimal sub-connected ZF beamformer \mathbb{B}_{ZF}^* is found by:

$$\mathcal{P}_4 : (\mathbb{B}_{\text{ZF}}^*, \mathcal{I}_{\text{ZF}}^*) = \underset{\mathbb{B}, \mathcal{I}}{\operatorname{argmax}} \{ \mathbf{R}_s^{\text{I}}(\mathbb{H}_{\mathbb{B},\mathcal{I}} + \mathbb{H}_{\mathbb{B},\mathcal{I}^c}\mathbb{B}^\top, \mathbb{H}_{\mathbb{E},\mathcal{I}} + \mathbb{H}_{\mathbb{E},\mathcal{I}^c}\mathbb{B}^\top) \} \quad (57)$$

$$\text{s.t.} \begin{cases} \|\mathbf{b}_j\|_1 \leq 1, \forall j, \\ |\mathbf{b}_j^\top \boldsymbol{\beta}_{\mathcal{I}} - \beta_{\mathcal{I}^c_j}| \leq \frac{1}{2} - \frac{1}{2}\|\mathbf{b}_j\|_1, \forall j, \\ \mathbb{H}_{\mathbb{E},\mathcal{I}^c}\mathbb{B}^\top = -\mathbb{H}_{\mathbb{E},\mathcal{I}}. \end{cases} \quad (58)$$

However, \mathcal{P}_4 may be infeasible. For example, if $\mathbb{H}_{\mathbb{E},\mathcal{I}^c}$ is full column-rank, we set $\mathbb{B} = (-\mathbb{H}_{\mathbb{E},\mathcal{I}^c}^\dagger \mathbb{H}_{\mathbb{E},\mathcal{I}})^\top$ to satisfy (56), where $\mathbb{H}_{\mathbb{E},\mathcal{I}^c}^\dagger = (\mathbb{H}_{\mathbb{E},\mathcal{I}^c}^\top \mathbb{H}_{\mathbb{E},\mathcal{I}^c})^{-1} \mathbb{H}_{\mathbb{E},\mathcal{I}^c}^\top$, is the Moore-Penrose inverse of $\mathbb{H}_{\mathbb{E},\mathcal{I}^c}$. If this \mathbb{B} violates the first two conditions in (58), i.e., the peak- and average-intensity constraints, then \mathcal{P}_4 has no feasible solution. To address this, we relax (56) and seek an approximate solution $\mathbb{B}_{\text{MLSE}}^*$ minimizing the least square error (MLSE) while satisfying the constraints:

$$\mathcal{P}_5 : (\mathbb{B}_{\text{MLSE}}^*, \mathcal{I}_{\text{MLSE}}^*) = \underset{\mathbb{B}, \mathcal{I}}{\operatorname{argmin}} \|\mathbb{H}_{\mathbb{E},\mathcal{I}^c}\mathbb{B}^\top + \mathbb{H}_{\mathbb{E},\mathcal{I}}\|_{\text{F}} \quad (59)$$

$$\text{s.t.} \begin{cases} \|\mathbf{b}_j\|_1 \leq 1, \forall j, \\ |\mathbf{b}_j^\top \boldsymbol{\beta}_{\mathcal{I}} - \beta_{\mathcal{I}^c_j}| \leq \frac{1}{2} - \frac{1}{2}\|\mathbf{b}_j\|_1, \forall j. \end{cases} \quad (60)$$

B. Beamforming Design for Case II

This section addresses Case II using analysis similar to Sec. IV-A1. The fully-connected beamforming scheme for Case II remains identical to (37) and Fig. 1(b). Using (11), the optimal fully-connected beamformer \mathbb{W}_{FC}^* maximizing the achievable secrecy rate is obtained by:

$$\mathcal{P}_6 : \mathbb{W}_{\text{FC}}^* = \underset{\mathbb{W}}{\operatorname{argmax}} \{ \mathbf{R}_s^{\text{II}}(\mathbb{H}_{\mathbb{B}}\mathbb{W}^\top, \mathbb{H}_{\mathbb{E}}\mathbb{W}^\top) \} \quad (61)$$

$$\text{s.t.} \begin{cases} \|\mathbf{w}_j\|_1 \leq 1, \forall j, \\ |\mathbf{w}_j^\top \boldsymbol{\beta} - \beta_j| \leq \frac{1}{2} - \frac{1}{2}\|\mathbf{w}_j\|_1, \forall j. \end{cases} \quad (62)$$

Note that under Case II, $\mathbb{H}_{\mathbb{E}}$ is a full column-rank matrix. The fully-connected ZF beamformer satisfying (43) corresponds to the zero matrix, rendering the ZF-based beamforming scheme infeasible. Furthermore, we observe that the sub-connected beamforming scheme degenerates to the direct-connected beamforming scheme. Specifically, with the

index set $\mathcal{I} = \{1, 2, \dots, n_{\text{T}}\}$, we obtain $\mathbb{H}_{\mathbb{B}} = \mathbb{H}_{\mathbb{B},\mathcal{I}}$. This configuration directly connects the j -th input X_j to the j LED for all $j \in \{1, \dots, n_{\text{T}}\}$, which corresponds precisely to the direct-connected beamforming scheme.

V. SECRECY RATE MAXIMIZATION ALGORITHM

This section develops efficient algorithms for solving the beamforming optimization problems \mathcal{P}_1 - \mathcal{P}_6 . Note that \mathcal{P}_1 - \mathcal{P}_6 (except \mathcal{P}_5) are non-convex due to non-concave objective functions. To address this challenge, we first decompose each problem's objective function into two components corresponding to the mutual information of Bob and Eve, respectively. For each component, we construct a strongly convex surrogate function: Bob's surrogate is derived from a second-order Taylor expansion with a positive semi-definite Hessian, while Eve's from a first-order Taylor expansion of a log-det function. These surrogates are then optimized within a successive convex approximation (SCA) framework, which has been proven to be effective in wireless communications, signal processing, and machine learning [42–44]. We begin by introducing SCA fundamentals before presenting SCA-based algorithms for the MIMO-VLC wiretap channel beamforming optimization.

A. Preliminary

Consider a non-convex problem:

$$\mathcal{P} : \min_{\mathbf{x} \in \mathcal{X}} f(\mathbf{x}), \quad (63)$$

where $f(\mathbf{x})$ is non-convex with respect to \mathbf{x} . For simplicity, we assume \mathcal{X} is a convex constraint. To solve such a non-convex problem, SCA first constructs a locally surrogate function to approximate $f(\mathbf{x})$ and then solves the difficult non-convex problem \mathcal{P} via successively solving a series of convex subproblems. Specifically, at k -th iteration, the subproblem for \mathcal{P} is given by

$$\mathcal{P}' : \hat{\mathbf{x}}^{(k+1)} = \underset{\mathbf{x} \in \mathcal{X}}{\operatorname{argmin}} \tilde{f}(\mathbf{x}; \mathbf{x}^{(k)}), \quad (64)$$

where $\mathbf{x}^{(k)}$ denotes the current iteration variable, and $\tilde{f}(\mathbf{x}; \mathbf{x}^{(k)})$ denotes the surrogate function of $f(\mathbf{x})$ at $\mathbf{x}^{(k)}$. The surrogate function $\tilde{f}(\mathbf{x}; \mathbf{x}^{(k)})$ is required to satisfy the following conditions:

- $\tilde{f}(\mathbf{x}^{(k)}; \mathbf{x}^{(k)}) = f(\mathbf{x}^{(k)})$;
- $\nabla \tilde{f}(\mathbf{x}^{(k)}; \mathbf{x}^{(k)}) = \nabla f(\mathbf{x}^{(k)})$;
- $\tilde{f}(\mathbf{x}; \mathbf{x}^{(k)})$ is strongly convex on \mathcal{X} .

The next iteration variable $\mathbf{x}^{(k+1)}$ is generated through

$$\mathbf{x}^{(k+1)} = \mathbf{x}^{(k)} + \gamma^{(k)}(\hat{\mathbf{x}}^{(k+1)} - \mathbf{x}^{(k)}), \quad (65)$$

where $\gamma^{(k)}$ is the step size at the k -th iteration. The convergence of SCA algorithm is guaranteed by $\lim_{k \rightarrow +\infty} \gamma^{(k)} = 0$ and $\sum_{k=0}^{+\infty} \gamma^{(k)} = +\infty$ [43, 44].

The key to the success of SCA lies in constructing the surrogate function at each iteration. In the following, we separately construct the surrogate functions for problems \mathcal{P}_1 - \mathcal{P}_6 (except \mathcal{P}_5) and propose the SCA-aided algorithms to solve them.

B. Algorithm for Case I

1) Fully-connected Beamforming Optimization Algorithm:

Note that the objective functions of problems \mathcal{P}_1 and \mathcal{P}_2 are the same, while their corresponding feasible domains are different. To be convenient, we denote the objective function of problem \mathcal{P}_1 or \mathcal{P}_2 by $-f(\mathbb{W})$, i.e.,

$$f(\mathbb{W}) = -\mathbf{R}_s^I(\mathbb{H}_B \mathbb{W}^T, \mathbb{H}_E \mathbb{W}^T). \quad (66)$$

Denote the feasible domain of problem \mathcal{P}_1 by \mathcal{W}_1 , and the feasible domain of problem \mathcal{P}_2 by \mathcal{W}_2 . Without ambiguity, the following algorithm applies to both \mathcal{P}_1 and \mathcal{P}_2 , and the difference is in the feasible domains.

To begin with, we divide $f(\mathbb{W})$ into two parts such that $f(\mathbb{W}) = f_B(\mathbb{W}) + f_E(\mathbb{W})$ with

$$f_B(\mathbb{W}) = -\frac{n_B}{2} \log \left(1 + \left| \mathbb{H}_B \mathbb{W}^T \cdot \text{diag}(\mathbf{p}) \cdot (\mathbb{H}_B \mathbb{W}^T)^T \right|^{\frac{1}{n_B}} \right), \quad (67)$$

$$f_E(\mathbb{W}) = \frac{1}{2} \log \left| \mathbb{H}_E \mathbb{W}^T \cdot \text{diag}(\mathbf{v}) \cdot (\mathbb{H}_E \mathbb{W}^T)^T + \mathbb{I}_{n_E} \right|, \quad (68)$$

where $f_B(\mathbb{W})$ corresponds to Bob and $f_E(\mathbb{W})$ to Eve. Then we separately construct the surrogate functions $\tilde{f}_B(\mathbb{W}; \mathbb{W}^{(k)})$ and $\tilde{f}_E(\mathbb{W}; \mathbb{W}^{(k)})$ for $f_B(\mathbb{W})$ and $f_E(\mathbb{W})$ such that

$$\tilde{f}(\mathbb{W}; \mathbb{W}^{(k)}) = \tilde{f}_B(\mathbb{W}; \mathbb{W}^{(k)}) + \tilde{f}_E(\mathbb{W}; \mathbb{W}^{(k)}). \quad (69)$$

For $f_B(\mathbb{W})$, we first characterize its gradient and Hessian matrix in the following lemma, whose proof is given in Appendix A.

Lemma 3:

$$\begin{aligned} \nabla f_B(\mathbb{W}) &= -\frac{|\mathbb{H}_B \mathbb{W}^T \cdot \text{diag}(\mathbf{p}) \cdot \mathbb{W} \mathbb{H}_B^T|^{\frac{1}{n_B}}}{1 + |\mathbb{H}_B \mathbb{W}^T \cdot \text{diag}(\mathbf{p}) \cdot \mathbb{W} \mathbb{H}_B^T|^{\frac{1}{n_B}}} \\ &\quad \cdot \text{diag}(\mathbf{p}) \cdot \mathbb{W} \mathbb{H}_B^T (\mathbb{H}_B \mathbb{W}^T \cdot \text{diag}(\mathbf{p}) \cdot \mathbb{W} \mathbb{H}_B^T)^{-1} \\ &\quad \cdot \mathbb{H}_B, \end{aligned} \quad (70)$$

$$\mathbb{G}_{f_B}(\mathbb{W}) = \mathbb{U}_1 \otimes \mathbb{V}_1 + \mathbb{K}_{n_T \times n_T} \cdot \mathbb{O}_1^T \otimes \mathbb{O}_1 - \mathbb{U}_2 \otimes \mathbb{V}_2, \quad (71)$$

where $\mathbb{K}_{n_T \times n_T}$ is the commutation matrix, and

$$\mathbb{U}_1 = \mathbb{U}_2 = \mathbb{H}_B^T (\mathbb{H}_B \mathbb{W}^T \cdot \text{diag}(\mathbf{p}) \cdot \mathbb{W} \mathbb{H}_B^T)^{-1} \mathbb{H}_B,$$

$$\mathbb{V}_1 = \text{diag}(\mathbf{p}) \cdot \mathbb{W} \mathbb{H}_B^T (\mathbb{H}_B \mathbb{W}^T \cdot \text{diag}(\mathbf{p}) \cdot \mathbb{W} \mathbb{H}_B^T)^{-1} \mathbb{H}_B \mathbb{W}^T \cdot \text{diag}(\mathbf{p}),$$

$$\mathbb{O}_1 = \mathbb{H}_B^T (\mathbb{H}_B \mathbb{W}^T \cdot \text{diag}(\mathbf{p}) \cdot \mathbb{W} \mathbb{H}_B^T)^{-1} \mathbb{H}_B \mathbb{W}^T \cdot \text{diag}(\mathbf{p}),$$

$$\mathbb{V}_2 = \text{diag}(\mathbf{p}). \quad \blacksquare$$

For convenience, we denote the Hessian matrix of $f_B(\mathbb{W})$ at $\mathbb{W}^{(k)}$ by $\mathbb{G}_{f_B}^{(k)}$. With Lemma 3, we construct $\tilde{f}_B(\mathbb{W}; \mathbb{W}^{(k)})$ based on the second-order Taylor expansion with a positive semi-definite Hessian matrix of $f_B(\mathbb{W})$ such that

$$\begin{aligned} \tilde{f}_B(\mathbb{W}; \mathbb{W}^{(k)}) &= f_B(\mathbb{W}^{(k)}) + \text{tr}\{\nabla f_B(\mathbb{W}^{(k)})^T (\mathbb{W} - \mathbb{W}^{(k)})\} \\ &\quad + \frac{1}{2} \text{vec}(\mathbb{W} - \mathbb{W}^{(k)})^T \hat{\mathbb{G}}_{f_B}^{(k)} \text{vec}(\mathbb{W} - \mathbb{W}^{(k)}), \end{aligned} \quad (72)$$

where $\hat{\mathbb{G}}_{f_B}^{(k)}$ is the nearest symmetric positive semi-definite matrix to $\mathbb{G}_{f_B}^{(k)}$, which achieves the minimum Frobenius-norm error, i.e., $\hat{\mathbb{G}}_{f_B}^{(k)} = \text{argmin}_{\mathbb{G}_{f_B} \in \mathcal{S}_+^n} \|\mathbb{G}_{f_B} - \mathbb{G}_{f_B}^{(k)}\|_F$ with $n = n_T^2$. It has been shown in [45] that if the eigenvalue decomposition of $\mathbb{G}_{f_B}^{(k)}$ is $\mathbb{G}_{f_B}^{(k)} = \mathbb{P} \cdot \text{diag}(\mathbf{h}) \cdot \mathbb{P}^T$, then $\hat{\mathbb{G}}_{f_B}^{(k)}$ can be formulated by $\hat{\mathbb{G}}_{f_B}^{(k)} = \mathbb{P} \cdot \text{diag}(\mathbf{h}_+) \cdot \mathbb{P}^T$, where $\mathbf{h} = (h_1, \dots, h_{n_T^2})^T$,

and $\mathbf{h}_+ = (h_1^+, \dots, h_{n_T^2}^+)^T$ with $h_i^+ = \begin{cases} h_i, & \text{if } h_i \geq 0, \\ 0, & \text{if } h_i < 0. \end{cases}$ To ensure that $\tilde{f}_B(\mathbb{W}; \mathbb{W}^{(k)})$ is strongly convex with respect to \mathbb{W} , we further include a second-order term to (72) such that

$$\begin{aligned} \tilde{f}_B(\mathbb{W}; \mathbb{W}^{(k)}) &= f_B(\mathbb{W}^{(k)}) + \text{tr}\{\nabla f_B(\mathbb{W}^{(k)})^T (\mathbb{W} - \mathbb{W}^{(k)})\} \\ &\quad + \frac{1}{2} \text{vec}(\mathbb{W} - \mathbb{W}^{(k)})^T \hat{\mathbb{G}}_{f_B}^{(k)} \text{vec}(\mathbb{W} - \mathbb{W}^{(k)}) \\ &\quad + \frac{\tau}{4} \|\mathbb{W} - \mathbb{W}^{(k)}\|_F^2, \end{aligned} \quad (73)$$

where $\tau > 0$.

For $f_E(\mathbb{W})$, we construct its surrogate function by combining the first-order Taylor expansion of the log-det function:

$$\log |\mathbb{X}| = \log |\mathbb{X}^{(k)}| + \text{tr}\{(\mathbb{X}^{(k)})^{-1} \cdot (\mathbb{X} - \mathbb{X}^{(k)})\}. \quad (74)$$

Substituting $\mathbb{X} = \mathbb{H}_E \mathbb{W}^T \cdot \text{diag}(\mathbf{v}) \cdot (\mathbb{H}_E \mathbb{W}^T)^T + \mathbb{I}_{n_E}$ and $\mathbb{X}^{(k)} = \mathbb{H}_E (\mathbb{W}^{(k)})^T \cdot \text{diag}(\mathbf{v}) \cdot (\mathbb{H}_E (\mathbb{W}^{(k)}))^T + \mathbb{I}_{n_E}$ into (74) and multiplying $\frac{1}{2}$ on both sides, we let

$$\begin{aligned} \tilde{f}_E(\mathbb{W}; \mathbb{W}^{(k)}) &= \frac{1}{2} \log \left| \mathbb{H}_E (\mathbb{W}^{(k)})^T \cdot \text{diag}(\mathbf{v}) \cdot (\mathbb{H}_E (\mathbb{W}^{(k)}))^T + \mathbb{I}_{n_E} \right| \\ &\quad + \frac{1}{2} \text{tr} \left\{ \left(\mathbb{H}_E (\mathbb{W}^{(k)})^T \cdot \text{diag}(\mathbf{v}) \cdot (\mathbb{H}_E (\mathbb{W}^{(k)}))^T + \mathbb{I}_{n_E} \right)^{-1} \right. \\ &\quad \left. \cdot \left(\mathbb{H}_E \mathbb{W}^T \cdot \text{diag}(\mathbf{v}) \cdot (\mathbb{H}_E \mathbb{W}^T)^T + \mathbb{I}_{n_E} \right) \right\} - \frac{n_E}{2}. \end{aligned} \quad (75)$$

Note that (75) is a convex function of \mathbb{W} . Similar to (73), we also include a second-order term to ensure that $\tilde{f}_E(\mathbb{W}; \mathbb{W}^{(k)})$ is strongly convex with respect to \mathbb{W} such that

$$\begin{aligned} \tilde{f}_E(\mathbb{W}; \mathbb{W}^{(k)}) &= \frac{1}{2} \log \left| \mathbb{H}_E (\mathbb{W}^{(k)})^T \cdot \text{diag}(\mathbf{v}) \cdot (\mathbb{H}_E (\mathbb{W}^{(k)}))^T + \mathbb{I}_{n_E} \right| \\ &\quad + \frac{1}{2} \text{tr} \left\{ \left(\mathbb{H}_E (\mathbb{W}^{(k)})^T \cdot \text{diag}(\mathbf{v}) \cdot (\mathbb{H}_E (\mathbb{W}^{(k)}))^T + \mathbb{I}_{n_E} \right)^{-1} \right. \\ &\quad \left. \cdot \left(\mathbb{H}_E \mathbb{W}^T \cdot \text{diag}(\mathbf{v}) \cdot (\mathbb{H}_E \mathbb{W}^T)^T + \mathbb{I}_{n_E} \right) \right\} \\ &\quad + \frac{\tau}{4} \|\mathbb{W} - \mathbb{W}^{(k)}\|_F^2 - \frac{n_E}{2}. \end{aligned} \quad (76)$$

Substituting (73) and (76) into (69), we can show that $\tilde{f}(\mathbb{W}; \mathbb{W}^{(k)}) = f(\mathbb{W}^{(k)})$, $\nabla \tilde{f}(\mathbb{W}; \mathbb{W}^{(k)}) = \nabla f(\mathbb{W}^{(k)})$, and the Hessian matrix of $\tilde{f}(\mathbb{W}; \mathbb{W}^{(k)})$ satisfies $\mathbb{G}_{\tilde{f}}(\mathbb{W}; \mathbb{W}^{(k)}) \succeq \tau \mathbb{I}_{n_T^2}$, indicating that $\tilde{f}(\mathbb{W}; \mathbb{W}^{(k)})$ is a strongly convex function. Therefore, the fully-connected beamforming optimization problem can be iteratively solved by the following convex subproblem:

$$\mathcal{P}'_{1\&2} : \hat{\mathbb{W}}^{(k+1)} = \underset{\mathbb{W} \in \mathcal{W}_i}{\text{argmin}} \tilde{f}(\mathbb{W}; \mathbb{W}^{(k)}), \quad (77)$$

where \mathcal{W}_i could be \mathcal{W}_1 or \mathcal{W}_2 , which corresponds to problem \mathcal{P}_1 or \mathcal{P}_2 , respectively. Besides, the next iteration variable $\mathbb{W}^{(k+1)}$ is generated similar to (65) such that

$$\mathbb{W}^{(k+1)} = \mathbb{W}^{(k)} + \gamma^{(k)} (\hat{\mathbb{W}}^{(k+1)} - \mathbb{W}^{(k)}). \quad (78)$$

We summarize the above proposed SCA-aided algorithm to solve \mathcal{P}_1 or \mathcal{P}_2 in the following.

Algorithm 1

- 1: Initialize $\mathbb{W}^{(0)}$, select a sequence $\{\gamma^{(k)}\}$;
 - 2: **for** $k = 0, 1, 2, \dots$ **do**
 - 3: Calculate $\nabla f_{\mathbb{B}}(\mathbb{W}^{(k)})$ in (70), $\mathbb{G}_{f_{\mathbb{B}}}^{(k)}$ in (71);
 - 4: Solve the problem (77) by CVX to obtain $\hat{\mathbb{W}}^{(k+1)}$;
 - 5: Update $\mathbb{W}^{(k+1)}$ by (78);
 - 6: Terminate loop if converges.
-

2) Sub-connected Beamforming Optimization Algorithm:

The procedure of solving problems \mathcal{P}_3 or \mathcal{P}_4 is similar to Sec. V-B1. Here we mainly emphasize the differences. Given a fixed \mathcal{I} satisfying $\mathcal{I} \in \mathcal{I}_{\text{all}}$, we also denote the objective function of problem \mathcal{P}_3 or \mathcal{P}_4 by $-f(\mathbb{B})$, i.e.,

$$f(\mathbb{B}) = -\mathbf{R}_s^l(\mathbb{H}_{\mathbb{B},\mathcal{I}} + \mathbb{H}_{\mathbb{B},\mathcal{I}^c}\mathbb{B}^T, \mathbb{H}_{\mathbb{E},\mathcal{I}} + \mathbb{H}_{\mathbb{E},\mathcal{I}^c}\mathbb{B}^T). \quad (79)$$

Denote the feasible domain of problem \mathcal{P}_3 by \mathcal{B}_1 , and the feasible domain of problem \mathcal{P}_4 by \mathcal{B}_2 . We divide $f(\mathbb{B})$ into two parts such that $f(\mathbb{B}) = f_{\mathbb{B}}(\mathbb{B}) + f_{\mathbb{E}}(\mathbb{B})$ with

$$f_{\mathbb{B}}(\mathbb{B}) = -\frac{n_{\mathbb{B}}}{2} \log\left(1 + |(\mathbb{H}_{\mathbb{B},\mathcal{I}} + \mathbb{H}_{\mathbb{B},\mathcal{I}^c}\mathbb{B}^T) \cdot \text{diag}(\mathbf{p}_{\mathcal{I}}) \cdot (\mathbb{H}_{\mathbb{B},\mathcal{I}} + \mathbb{H}_{\mathbb{B},\mathcal{I}^c}\mathbb{B}^T)^T|^{\frac{1}{n_{\mathbb{B}}}}\right), \quad (80)$$

$$f_{\mathbb{E}}(\mathbb{B}) = \frac{1}{2} \log\left|(\mathbb{H}_{\mathbb{E},\mathcal{I}} + \mathbb{H}_{\mathbb{E},\mathcal{I}^c}\mathbb{B}^T) \cdot \text{diag}(\mathbf{v}_{\mathcal{I}}) \cdot (\mathbb{H}_{\mathbb{E},\mathcal{I}} + \mathbb{H}_{\mathbb{E},\mathcal{I}^c}\mathbb{B}^T)^T + \mathbb{I}_{n_{\mathbb{E}}}\right|, \quad (81)$$

where $\mathbf{p}_{\mathcal{I}}$ and $\mathbf{v}_{\mathcal{I}}$ denote the subvectors of \mathbf{p} and \mathbf{v} with entries indexed by \mathcal{I} , respectively.

For $f_{\mathbb{B}}(\mathbb{B})$, its gradient and Hessian matrix are given in the following lemma whose proof is similar to Appendix A and omitted.

Lemma 4:

$$\begin{aligned} \nabla f_{\mathbb{B}}(\mathbb{B}) &= -\frac{|(\mathbb{H}_{\mathbb{B},\mathcal{I}} + \mathbb{H}_{\mathbb{B},\mathcal{I}^c}\mathbb{B}^T) \cdot \text{diag}(\mathbf{p}_{\mathcal{I}}) \cdot (\mathbb{H}_{\mathbb{B},\mathcal{I}} + \mathbb{H}_{\mathbb{B},\mathcal{I}^c}\mathbb{B}^T)^T|^{\frac{1}{n_{\mathbb{B}}}}}{1 + |(\mathbb{H}_{\mathbb{B},\mathcal{I}} + \mathbb{H}_{\mathbb{B},\mathcal{I}^c}\mathbb{B}^T) \cdot \text{diag}(\mathbf{p}_{\mathcal{I}}) \cdot (\mathbb{H}_{\mathbb{B},\mathcal{I}} + \mathbb{H}_{\mathbb{B},\mathcal{I}^c}\mathbb{B}^T)^T|^{\frac{1}{n_{\mathbb{B}}}} \cdot \text{diag}(\mathbf{p}_{\mathcal{I}}) \cdot (\mathbb{H}_{\mathbb{B},\mathcal{I}} + \mathbb{H}_{\mathbb{B},\mathcal{I}^c}\mathbb{B}^T)^T} \left((\mathbb{H}_{\mathbb{B},\mathcal{I}} + \mathbb{H}_{\mathbb{B},\mathcal{I}^c}\mathbb{B}^T) \right. \\ &\quad \left. \cdot \text{diag}(\mathbf{p}_{\mathcal{I}}) \cdot (\mathbb{H}_{\mathbb{B},\mathcal{I}} + \mathbb{H}_{\mathbb{B},\mathcal{I}^c}\mathbb{B}^T)^T \right)^{-1} \mathbb{H}_{\mathbb{B},\mathcal{I}^c}, \end{aligned} \quad (82)$$

$$\mathbb{G}_{f_{\mathbb{B}}}(\mathbb{B}) = \mathbb{U}_3 \otimes \mathbb{V}_3 + \mathbb{K}_{(n_{\mathbb{T}}-n_{\mathbb{B}}) \times n_{\mathbb{B}}} \cdot \mathbb{O}_2^T \otimes \mathbb{O}_2 - \mathbb{U}_4 \otimes \mathbb{V}_4, \quad (83)$$

where

$$\begin{aligned} \mathbb{U}_3 &= \mathbb{U}_4 = \mathbb{H}_{\mathbb{B},\mathcal{I}^c}^T \left((\mathbb{H}_{\mathbb{B},\mathcal{I}} + \mathbb{H}_{\mathbb{B},\mathcal{I}^c}\mathbb{B}^T) \cdot \text{diag}(\mathbf{p}_{\mathcal{I}}) \cdot (\mathbb{H}_{\mathbb{B},\mathcal{I}} + \mathbb{H}_{\mathbb{B},\mathcal{I}^c}\mathbb{B}^T)^T \right)^{-1} \mathbb{H}_{\mathbb{B},\mathcal{I}^c}, \\ \mathbb{V}_3 &= \text{diag}(\mathbf{p}_{\mathcal{I}}) \cdot (\mathbb{H}_{\mathbb{B},\mathcal{I}} + \mathbb{H}_{\mathbb{B},\mathcal{I}^c}\mathbb{B}^T)^T \left((\mathbb{H}_{\mathbb{B},\mathcal{I}} + \mathbb{H}_{\mathbb{B},\mathcal{I}^c}\mathbb{B}^T) \cdot \text{diag}(\mathbf{p}_{\mathcal{I}}) \cdot (\mathbb{H}_{\mathbb{B},\mathcal{I}} + \mathbb{H}_{\mathbb{B},\mathcal{I}^c}\mathbb{B}^T)^T \right)^{-1} (\mathbb{H}_{\mathbb{B},\mathcal{I}} + \mathbb{H}_{\mathbb{B},\mathcal{I}^c}\mathbb{B}^T) \\ &\quad \cdot \text{diag}(\mathbf{p}_{\mathcal{I}}), \\ \mathbb{O}_2 &= \mathbb{H}_{\mathbb{B},\mathcal{I}^c}^T \left((\mathbb{H}_{\mathbb{B},\mathcal{I}} + \mathbb{H}_{\mathbb{B},\mathcal{I}^c}\mathbb{B}^T) \cdot \text{diag}(\mathbf{p}_{\mathcal{I}}) \cdot (\mathbb{H}_{\mathbb{B},\mathcal{I}} + \mathbb{H}_{\mathbb{B},\mathcal{I}^c}\mathbb{B}^T)^T \right)^{-1} (\mathbb{H}_{\mathbb{B},\mathcal{I}} + \mathbb{H}_{\mathbb{B},\mathcal{I}^c}\mathbb{B}^T) \cdot \text{diag}(\mathbf{p}_{\mathcal{I}}), \\ \mathbb{V}_4 &= \text{diag}(\mathbf{p}_{\mathcal{I}}). \end{aligned} \quad \blacksquare$$

Combined with Lemma 4, we let

$$\begin{aligned} \tilde{f}_{\mathbb{B}}(\mathbb{B}; \mathbb{B}^{(k)}) &= f_{\mathbb{B}}(\mathbb{B}^{(k)}) + \text{tr}\{\nabla f_{\mathbb{B}}(\mathbb{B}^{(k)})^T (\mathbb{B} - \mathbb{B}^{(k)})\} \\ &\quad + \frac{1}{2} \text{vec}(\mathbb{B} - \mathbb{B}^{(k)})^T \hat{\mathbb{G}}_{f_{\mathbb{B}}}^{(k)} \text{vec}(\mathbb{B} - \mathbb{B}^{(k)}) \\ &\quad + \frac{\tau}{4} \|\mathbb{B} - \mathbb{B}^{(k)}\|_{\mathbb{F}}^2, \end{aligned} \quad (84)$$

where $\mathbb{G}_{f_{\mathbb{B}}}^{(k)}$ is the Hessian matrix of $f_{\mathbb{B}}(\mathbb{B})$ at $\mathbb{B}^{(k)}$, and $\hat{\mathbb{G}}_{f_{\mathbb{B}}}^{(k)}$ is the nearest symmetric positive semi-definite matrix to $\mathbb{G}_{f_{\mathbb{B}}}^{(k)}$ achieving the minimum Frobenius-norm error.

For $f_{\mathbb{E}}(\mathbb{B})$, we substitute $\mathbb{X} = (\mathbb{H}_{\mathbb{E},\mathcal{I}} + \mathbb{H}_{\mathbb{E},\mathcal{I}^c}\mathbb{B}^T) \cdot \text{diag}(\mathbf{v}_{\mathcal{I}}) \cdot (\mathbb{H}_{\mathbb{E},\mathcal{I}} + \mathbb{H}_{\mathbb{E},\mathcal{I}^c}\mathbb{B}^T)^T + \mathbb{I}_{n_{\mathbb{E}}}$ and $\mathbb{X}^{(k)} = (\mathbb{H}_{\mathbb{E},\mathcal{I}} + \mathbb{H}_{\mathbb{E},\mathcal{I}^c}(\mathbb{B}^{(k)})^T) \cdot \text{diag}(\mathbf{v}_{\mathcal{I}}) \cdot (\mathbb{H}_{\mathbb{E},\mathcal{I}} + \mathbb{H}_{\mathbb{E},\mathcal{I}^c}(\mathbb{B}^{(k)})^T)^T + \mathbb{I}_{n_{\mathbb{E}}}$ into (74), and let

$$\begin{aligned} \tilde{f}_{\mathbb{E}}(\mathbb{B}; \mathbb{B}^{(k)}) &= \frac{1}{2} \log\left|(\mathbb{H}_{\mathbb{E},\mathcal{I}} + \mathbb{H}_{\mathbb{E},\mathcal{I}^c}(\mathbb{B}^{(k)})^T) \cdot \text{diag}(\mathbf{v}_{\mathcal{I}}) \cdot (\mathbb{H}_{\mathbb{E},\mathcal{I}} + \mathbb{H}_{\mathbb{E},\mathcal{I}^c}(\mathbb{B}^{(k)})^T)^T + \mathbb{I}_{n_{\mathbb{E}}}\right| \\ &\quad + \frac{1}{2} \text{tr}\left\{\left((\mathbb{H}_{\mathbb{E},\mathcal{I}} + \mathbb{H}_{\mathbb{E},\mathcal{I}^c}(\mathbb{B}^{(k)})^T) \cdot \text{diag}(\mathbf{v}_{\mathcal{I}}) \cdot (\mathbb{H}_{\mathbb{E},\mathcal{I}} + \mathbb{H}_{\mathbb{E},\mathcal{I}^c}(\mathbb{B}^{(k)})^T)^T + \mathbb{I}_{n_{\mathbb{E}}}\right)^{-1} \cdot \left((\mathbb{H}_{\mathbb{E},\mathcal{I}} + \mathbb{H}_{\mathbb{E},\mathcal{I}^c}\mathbb{B}^T) \cdot \text{diag}(\mathbf{v}_{\mathcal{I}}) \cdot (\mathbb{H}_{\mathbb{E},\mathcal{I}} + \mathbb{H}_{\mathbb{E},\mathcal{I}^c}\mathbb{B}^T)^T + \mathbb{I}_{n_{\mathbb{E}}}\right)\right\} \\ &\quad + \frac{\tau}{4} \|\mathbb{B} - \mathbb{B}^{(k)}\|_{\mathbb{F}}^2 - \frac{n_{\mathbb{E}}}{2}. \end{aligned} \quad (85)$$

As a result, we construct the surrogate function $\tilde{f}(\mathbb{B}; \mathbb{B}^{(k)})$ for $f(\mathbb{B})$ at k -th iteration by

$$\tilde{f}(\mathbb{B}; \mathbb{B}^{(k)}) = \tilde{f}_{\mathbb{B}}(\mathbb{B}; \mathbb{B}^{(k)}) + \tilde{f}_{\mathbb{E}}(\mathbb{B}; \mathbb{B}^{(k)}). \quad (86)$$

Combining (84) and (85), we can show that the Hessian matrix of $\tilde{f}(\mathbb{B}; \mathbb{B}^{(k)})$ satisfies $\mathbb{G}_{\tilde{f}}(\mathbb{B}; \mathbb{B}^{(k)}) \succcurlyeq \tau \mathbb{I}_{n_{\mathbb{B}} \cdot (n_{\mathbb{T}} - n_{\mathbb{B}})}, \forall \mathbb{B} \in \mathcal{B}_i$. Therefore, the strongly convex subproblem at k iteration is given by

$$\mathcal{P}'_{3\&4} : \hat{\mathbb{B}}^{(k+1)} = \underset{\mathbb{B} \in \mathcal{B}_i}{\text{argmin}} \tilde{f}(\mathbb{B}; \mathbb{B}^{(k)}), \quad (87)$$

where \mathcal{B}_i could be \mathcal{B}_1 or \mathcal{B}_2 . And the next iteration variable $\mathbb{B}^{(k+1)}$ is generated by

$$\mathbb{B}^{(k+1)} = \mathbb{B}^{(k)} + \gamma^{(k)} (\hat{\mathbb{B}}^{(k+1)} - \mathbb{B}^{(k)}). \quad (88)$$

We summarize the above proposed SCA-aided algorithm for problem \mathcal{P}_3 or \mathcal{P}_4 in the following.

Algorithm 2

- 1: **for** $\mathcal{I} \in \mathcal{I}_{\text{all}}$ **do**
 - 2: Initialize $\mathbb{B}^{(0)}$, select a sequence $\{\gamma^{(k)}\}$;
 - 3: **for** $k = 0, 1, 2, \dots$ **do**
 - 4: Calculate $\nabla f_{\mathbb{B}}(\mathbb{B}^{(k)})$ in (82), $\mathbb{G}_{f_{\mathbb{B}}}^{(k)}$ in (83);
 - 5: Solve the problem (87) by CVX to obtain $\hat{\mathbb{B}}^{(k+1)}$;
 - 6: Update $\mathbb{B}^{(k+1)}$ by (88);
 - 7: Terminate loop if converges;
 - 8: **end**
 - 9: Save $\mathbb{B}^{(k+1)}$ as $\mathbb{B}_{\mathcal{I}}$;
 - 10: **end**
 - 11: Output the optimal beamformer \mathbb{B}^* among $\mathbb{B}_{\mathcal{I}}$ s, $\mathcal{I} \in \mathcal{I}_{\text{all}}$.
-

C. Algorithm for Case II

For problem \mathcal{P}_6 , we also denote its objective function by $-f(\mathbb{W})$ and feasible domain by \mathcal{W}_3 . Similarly, We expand $f(\mathbb{W}) = f_B(\mathbb{W}) + f_E(\mathbb{W})$ with

$$f_B(\mathbb{W}) = -\frac{n_T}{2} \log\left(1 + |\text{diag}(\mathbf{p})|^{\frac{1}{n_T}} \cdot |\mathbb{W}\mathbb{H}_B^T\mathbb{H}_B\mathbb{W}^T|^{\frac{1}{n_T}}\right), \quad (89)$$

$$f_E(\mathbb{W}) = \frac{1}{2} \log|\text{diag}(\mathbf{v}) \cdot \mathbb{W}\mathbb{H}_E^T\mathbb{H}_E\mathbb{W}^T + \mathbb{I}_{n_T}|. \quad (90)$$

For $f_B(\mathbb{W})$, its gradient and Hessian matrix are given in the following lemma whose proof is similar to Appendix A and omitted.

Lemma 5:

$$\nabla f_B(\mathbb{W}) = -\frac{|\text{diag}(\mathbf{p})|^{\frac{1}{n_T}} |\mathbb{W}\mathbb{H}_B^T\mathbb{H}_B\mathbb{W}^T|^{\frac{1}{n_T}}}{1 + |\text{diag}(\mathbf{p})|^{\frac{1}{n_T}} |\mathbb{W}\mathbb{H}_B^T\mathbb{H}_B\mathbb{W}^T|^{\frac{1}{n_T}}} \cdot (\mathbb{W}\mathbb{H}_B^T\mathbb{H}_B\mathbb{W}^T)^{-1} \mathbb{W}\mathbb{H}_B^T\mathbb{H}_B, \quad (91)$$

$$\mathbb{G}_{f_B}(\mathbb{W}) = -\mathbb{U}_5 \otimes \mathbb{V}_5 + \mathbb{K}_{n_T \times n_T} \cdot \mathbb{O}_3^T \otimes \mathbb{O}_3 + \mathbb{U}_6 \otimes \mathbb{V}_6, \quad (92)$$

where

$$\mathbb{U}_5 = \mathbb{H}_B^T\mathbb{H}_B,$$

$$\mathbb{V}_5 = \mathbb{V}_6 = (\mathbb{W}\mathbb{H}_B^T\mathbb{H}_B\mathbb{W}^T)^{-1},$$

$$\mathbb{O}_3 = \mathbb{H}_B^T\mathbb{H}_B\mathbb{W}^T(\mathbb{W}\mathbb{H}_B^T\mathbb{H}_B\mathbb{W}^T)^{-1},$$

$$\mathbb{U}_6 = \mathbb{H}_B^T\mathbb{H}_B\mathbb{W}^T(\mathbb{W}\mathbb{H}_B^T\mathbb{H}_B\mathbb{W}^T)^{-1}\mathbb{W}\mathbb{H}_B^T\mathbb{H}_B. \quad \blacksquare$$

Combined with Lemma 5, we design

$$\begin{aligned} \tilde{f}_B(\mathbb{W}; \mathbb{W}^{(k)}) &= f_B(\mathbb{W}^{(k)}) + \text{tr}\{\nabla f_B(\mathbb{W}^{(k)})^T(\mathbb{W} - \mathbb{W}^{(k)})\} \\ &\quad + \frac{1}{2} \text{vec}(\mathbb{W} - \mathbb{W}^{(k)})^T \hat{\mathbb{G}}_{f_B}^{(k)} \text{vec}(\mathbb{W} - \mathbb{W}^{(k)}) \\ &\quad + \frac{\tau}{4} \|\mathbb{W} - \mathbb{W}^{(k)}\|_F^2, \end{aligned} \quad (93)$$

where $\mathbb{G}_{f_B}^{(k)}$ is the Hessian matrix of $f_B(\mathbb{W})$ at $\mathbb{W}^{(k)}$, and $\hat{\mathbb{G}}_{f_B}^{(k)}$ is the nearest symmetric positive semi-definite matrix to $\mathbb{G}_{f_B}^{(k)}$ achieving the minimum Frobenius-norm error.

For $f_E(\mathbb{W})$, we let

$$\begin{aligned} \tilde{f}_E(\mathbb{W}; \mathbb{W}^{(k)}) &= \frac{1}{2} \log|\text{diag}(\mathbf{v}) \cdot \mathbb{W}^{(k)}\mathbb{H}_E^T\mathbb{H}_E(\mathbb{W}^{(k)})^T + \mathbb{I}_{n_T}| \\ &\quad + \frac{1}{2} \text{tr}\left\{ \left(\text{diag}(\mathbf{v}) \cdot \mathbb{W}^{(k)}\mathbb{H}_E^T\mathbb{H}_E(\mathbb{W}^{(k)})^T + \mathbb{I}_{n_T} \right)^{-1} \right. \\ &\quad \left. \cdot \left(\text{diag}(\mathbf{v}) \cdot \mathbb{W}\mathbb{H}_E^T\mathbb{H}_E\mathbb{W}^T + \mathbb{I}_{n_T} \right) \right\} \\ &\quad + \frac{\tau}{4} \|\mathbb{W} - \mathbb{W}^{(k)}\|_F^2 - \frac{n_T}{2}. \end{aligned} \quad (94)$$

We construct the surrogate function $\tilde{f}(\mathbb{W}; \mathbb{W}^{(k)})$ for $f(\mathbb{W})$ by

$$\tilde{f}(\mathbb{W}; \mathbb{W}^{(k)}) = \tilde{f}_B(\mathbb{W}; \mathbb{W}^{(k)}) + \tilde{f}_E(\mathbb{W}; \mathbb{W}^{(k)}), \quad (95)$$

Then, the strongly convex subproblem at k iteration is

$$\mathcal{P}'_6 : \hat{\mathbb{W}}^{(k+1)} = \underset{\mathbb{W} \in \mathcal{W}_3}{\text{argmin}} \tilde{f}(\mathbb{W}; \mathbb{W}^{(k)}). \quad (96)$$

And the next iteration variable $\mathbb{W}^{(k+1)}$ is generated similar to (78). The proposed SCA-aided algorithm for problem \mathcal{P}_6 is summarized as follows.

Algorithm 3

- 1: Initialize $\mathbb{W}^{(0)}$, select a sequence $\{\gamma^{(k)}\}$;
 - 2: **for** $k = 0, 1, 2, \dots$ **do**
 - 3: Calculate $\nabla f_B(\mathbb{W}^{(k)})$ in (91), $\mathbb{G}_{f_B}^{(k)}$ in (92);
 - 4: Solve the problem (96) by CVX to obtain $\hat{\mathbb{W}}^{(k+1)}$;
 - 5: Update $\mathbb{W}^{(k+1)}$ by (78);
 - 6: Terminate loop if converges.
-

D. Complexity Analysis

Since the proposed Algorithms 1-3 are all iterative methods, we only discuss the computational complexity in constructing the convex subproblem at each iteration (note that the whole computational complexity of solving such a subproblem depends on the specific CVX solver). For Algorithm 1, the main computational costs are from computing the gradient $\nabla f_B(\mathbb{W}^{(k)})$ and Hessian matrix $\mathbb{G}_{f_B}^{(k)}$, which are $\mathcal{O}(n_B n_T^2)$ and $\mathcal{O}(n_T^4)$, respectively. For Algorithm 2, the computational costs of computing the gradient $\nabla f_B(\mathbb{W}^{(k)})$ and Hessian matrix $\mathbb{G}_{f_B}^{(k)}$ are $\mathcal{O}(n_B^3 + n_B^2(n_T - n_B))$ and $\mathcal{O}(n_B^2(n_T - n_B)^2)$, respectively. For Algorithm 3, the computational costs of computing the gradient $\nabla f_B(\mathbb{W}^{(k)})$ and Hessian matrix $\mathbb{G}_{f_B}^{(k)}$ are $\mathcal{O}(n_T n_B^2)$ and $\mathcal{O}(n_T^4)$, respectively.

VI. SIMULATION RESULTS

This section presents simulations evaluating the achievable secrecy rates under various system configurations. First, the analytical expressions derived in Thm. 2 are validated by comparing them against prior work considering a single peak-intensity constraint. Subsequently, the achievable secrecy rates under both peak- and average-intensity constraints are examined, and the performance gains achieved by the proposed beamforming schemes are demonstrated. For clarity and reproducibility, two sets of randomly generated channel matrices are considered in the simulations, i.e.,

- Group 1:

$$\mathbb{H}_B^{1 \times 4} = \begin{pmatrix} 0.8143 & 0.2435 & 0.9293 & 0.3500 \end{pmatrix}, \quad (97)$$

$$\mathbb{H}_E^{1 \times 4} = \begin{pmatrix} 0.3034 & 0.2489 & 0.1160 & 0.0267 \end{pmatrix}; \quad (98)$$

- Group 2:

$$\mathbb{H}_B^{2 \times 4} = \begin{pmatrix} 0.9218 & 1.2922 & 1.1557 & 1.3491 \\ 1.4157 & 1.4595 & 0.5357 & 1.4340 \end{pmatrix}, \quad (99)$$

$$\mathbb{H}_E^{2 \times 4} = \begin{pmatrix} 0.1787 & 0.2431 & 0.1555 & 0.2060 \\ 0.2577 & 0.1078 & 0.3288 & 0.4682 \end{pmatrix}. \quad (100)$$

A. Single Peak-intensity Constraint

When $\alpha_i = 0.5$ for all i , the average-intensity constraint becomes inactive [11, 34, 35], and the considered system reduces to a scenario with a single peak-intensity constraint. Under this setting, Fig. 3 compares the achievable secrecy rates from Thm. 2 at $\alpha_i = 0.5$ with those reported in prior works [14, 33],⁷ both of which consider a single peak-intensity

⁷For Fig. 3(b), simulations adopt the parameters specified in [33], i.e., “ $K_u = \frac{n_{TX}}{L}$, $\alpha = \Lambda$, $\beta = 2$ ”.

constraint (with [14] focusing on the MISO channel and [33] on the MIMO channel).

As shown in Fig. 3(a), the secrecy rate in Thm. 2 at $\alpha_i = 0.5$ aligns with that of [14], thereby validating the correctness of the derived analytical expression. Furthermore, a comparative analysis of Fig. 3(a) and Fig. 3(b) reveals distinct performance trends across the SNR range. At low SNR, the achievable secrecy rate in [33] exceeds that of both Thm. 2 and [14]. In contrast, at high SNR, Thm. 2 outperforms [33], yielding a strictly higher secrecy rate. These performance trends are attributable to the distinct input distributions employed. Specifically, [14] and Thm. 2 leverage a uniform distribution (as the truncated exponential distribution in (7) degenerates to a uniform distribution when $\alpha_i = 0.5$), whereas [33] adopts a discrete distribution. As established in [11], for peak-intensity-constrained channels, the optimal input distribution is discrete at low SNR but converges to a uniform distribution at high SNR. This theoretical insight fully accounts for the observed behaviors illustrated in Fig. 3.

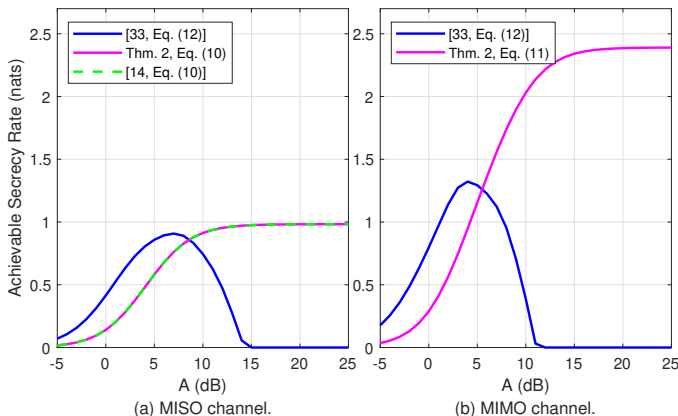


Fig. 3: Comparison of achievable secrecy rates: (a). $\mathbb{H}_B = \mathbb{H}_B^{1 \times 4}$ and $\mathbb{H}_E = \mathbb{H}_E^{1 \times 4}$; (b). $\mathbb{H}_B = (\mathbb{H}_B^{2 \times 4})^T$ and $\mathbb{H}_E = (\mathbb{H}_E^{2 \times 4})^T$.

B. Both Peak- and Average-intensity Constraints

1) Fully-connected Beamforming Schemes in \mathcal{P}_1 and \mathcal{P}_2 :

We employ Algorithm 1 to solve the fully-connected beamforming optimization problems \mathcal{P}_1 and \mathcal{P}_2 . To do it, we initialize $\mathbb{W}^{(0)} = \begin{pmatrix} \mathbb{I}_{n_B} & \mathbf{0}_{n_B \times (n_T - n_B)} \\ \mathbf{0}_{(n_T - n_B) \times n_B} & \mathbf{0}_{(n_T - n_B) \times (n_T - n_B)} \end{pmatrix}$, $\tau = 10^{-5}$, and $\gamma^{(0)} = 1$. During each iteration, we update the sequence $\{\gamma^{(k)}\}$ by:⁸

$$\gamma^{(k+1)} = \gamma^{(k)} \left(1 - 10^{-2} \gamma^{(k)}\right). \quad (101)$$

The algorithm is terminated if any of the following conditions is satisfied:

$$\begin{cases} \|\mathbb{W}^{(k+1)} - \mathbb{W}^{(k)}\|_F \leq 10^{-6}, \\ |f(\mathbb{W}^{(k+1)}) - f(\mathbb{W}^{(k)})| \leq 10^{-6}. \end{cases} \quad (102)$$

Figs. 4 and 5 illustrate the secrecy rates achieved by the optimal fully-connected beamformer \mathbb{W}_{FC}^* in \mathcal{P}_1 and the

⁸It should be noted that $\mathbb{W}^{(0)}$ is not necessarily a feasible point in \mathcal{W}_i , $i \in \{1, 2\}$. This is because the iteration variable $\mathbb{W}^{(1)}$ must be feasible by (78) since $\gamma^{(0)} = 1$.

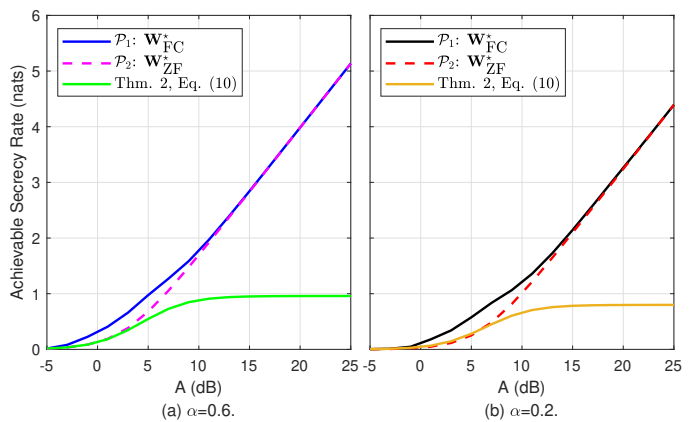


Fig. 4: Achievable secrecy rates of fully-connected beamformer when $\mathbb{H}_B = \mathbb{H}_B^{1 \times 4}$, $\mathbb{H}_E = \mathbb{H}_E^{1 \times 4}$, and $\alpha = \alpha \mathbf{1}_4$.

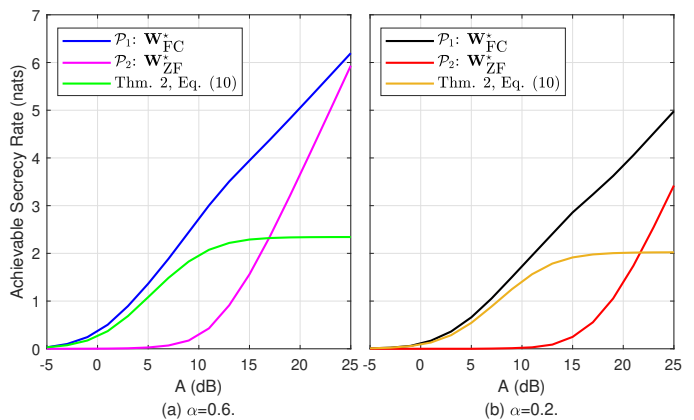


Fig. 5: Achievable secrecy rates of fully-connected beamformer when $\mathbb{H}_B = \mathbb{H}_B^{2 \times 4}$, $\mathbb{H}_E = \mathbb{H}_E^{2 \times 4}$, and $\alpha = \alpha \mathbf{1}_4$.

optimal fully-connected ZF beamformer \mathbb{W}_{ZF}^* in \mathcal{P}_2 . Here, an MISO channel corresponds to Fig. 4, and an MIMO channel corresponds to Fig. 5. To assess the effectiveness of the proposed beamforming design, the achievable secrecy rates are compared with those derived in Thm. 2, which corresponds to a direct-connected scheme without beamforming.

As shown in Fig. 4, both \mathbb{W}_{FC}^* and \mathbb{W}_{ZF}^* significantly enhance the secrecy rate compared to the direct-connected beamformer, thereby highlighting the potential secrecy gains through beamforming in practical VLC systems. Moreover, Fig. 4 reveals that for the MISO-VLC wiretap channel, \mathbb{W}_{FC}^* and \mathbb{W}_{ZF}^* exhibit nearly identical performance at high SNR, which is consistent with the observations in [14]. From Fig. 5, it is further observed that imposing the ZF constraint leads to a slight secrecy performance degradation compared with the unconstrained fully-connected scheme. Nevertheless, the ZF beamformer still substantially outperforms the direct-connected beamformer at high SNR, thereby demonstrating the effectiveness of the proposed ZF beamforming scheme.

2) *Sub-connected Beamforming Schemes in \mathcal{P}_3 , \mathcal{P}_4 and \mathcal{P}_5 :* We apply Algorithm 2 to solve the sub-connected beamforming optimization problems \mathcal{P}_3 and \mathcal{P}_4 , whereas the convex problem \mathcal{P}_5 is solved using CVX. The algorithm is initialized by: $\mathbb{B}^{(0)} = \mathbf{0}_{n_B \times (n_T - n_B)}$, and terminated if any of the

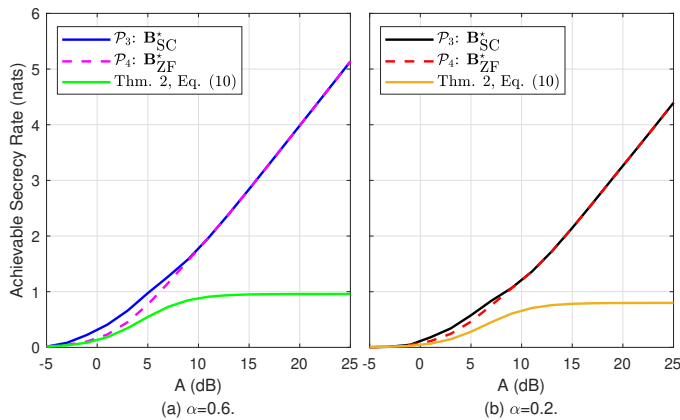


Fig. 6: Achievable secrecy rates of sub-connected beamformer when $\mathbb{H}_B = \mathbb{H}_B^{1 \times 4}$, $\mathbb{H}_E = \mathbb{H}_E^{1 \times 4}$, and $\alpha = \alpha \mathbf{1}_4$.

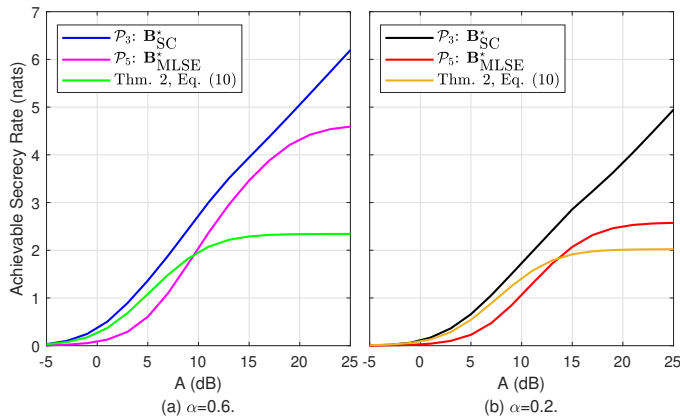


Fig. 7: Achievable secrecy rates of sub-connected beamformer when $\mathbb{H}_B = \mathbb{H}_B^{2 \times 4}$, $\mathbb{H}_E = \mathbb{H}_E^{2 \times 4}$, and $\alpha = \alpha \mathbf{1}_4$.

following conditions is satisfied:

$$\begin{cases} \|\mathbb{B}^{(k+1)} - \mathbb{B}^{(k)}\|_F \leq 10^{-6}, \\ |f(\mathbb{B}^{(k+1)}) - f(\mathbb{B}^{(k)})| \leq 10^{-6}. \end{cases} \quad (103)$$

Figs. 6 and 7 depict the secrecy rates achieved by the optimal sub-connected beamformer \mathbb{B}_{SC}^* in \mathcal{P}_3 , the optimal sub-connected ZF beamformer \mathbb{B}_{ZF}^* in \mathcal{P}_4 , and the optimal sub-connected MLSE beamformer \mathbb{B}_{MLSE}^* in \mathcal{P}_5 . Here, Fig. 6 refers to an MISO channel, and Fig. 7 refers to an MIMO channel.

As shown in Fig. 6, both \mathbb{B}_{SC}^* and \mathbb{B}_{ZF}^* achieve notable improvements in secrecy rate over the direct-connected beamformer, thereby confirming the effectiveness of sub-connected beamforming for enhancing physical-layer security. Similar to observations in Fig. 4, \mathbb{B}_{SC}^* and \mathbb{B}_{ZF}^* achieve identical secrecy performance at high SNR for the MISO channel, indicating that the ZF constraint incurs no performance loss asymptotically. From Fig. 7, we observe that for the MIMO-VLC wiretap channel, the MLSE-based beamformer \mathbb{B}_{MLSE}^* consistently outperforms the direct-connected beamformer as the SNR increases. This result highlights the advantage of incorporating MLSE beamforming in sub-connected architectures, particularly in scenarios where the ZF structure is impractical due to constraints.

3) *Comparison between Fully-connected and Sub-connected Beamforming Schemes in \mathcal{P}_1 and \mathcal{P}_3* : Figs. 8 and

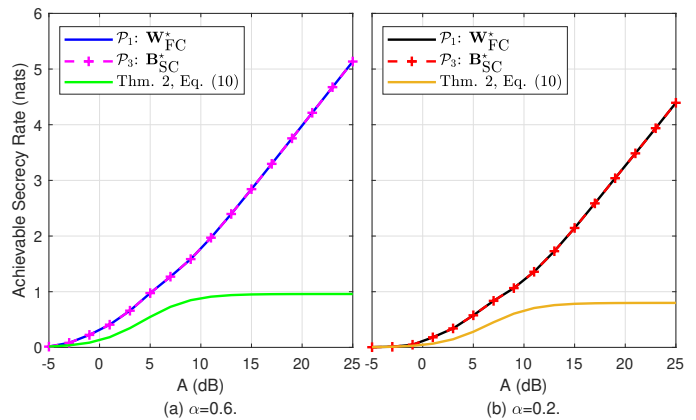


Fig. 8: Comparison between fully- and sub-connected beamformers when $\mathbb{H}_B = \mathbb{H}_B^{1 \times 4}$, $\mathbb{H}_E = \mathbb{H}_E^{1 \times 4}$, and $\alpha = \alpha \mathbf{1}_4$.

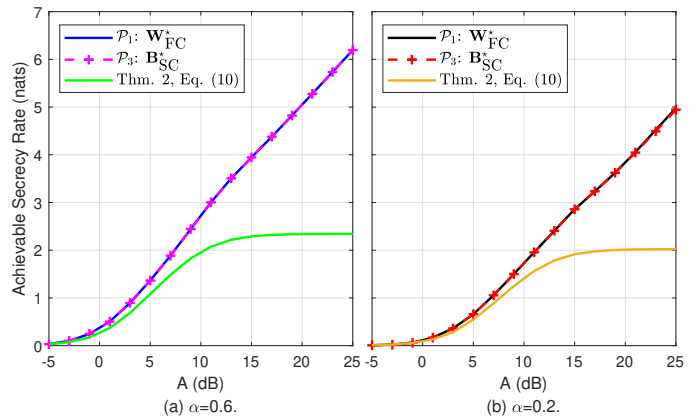


Fig. 9: Comparison between fully- and sub-connected beamformers when $\mathbb{H}_B = \mathbb{H}_B^{2 \times 4}$, $\mathbb{H}_E = \mathbb{H}_E^{2 \times 4}$, and $\alpha = \alpha \mathbf{1}_4$.

9 compare the secrecy rates achieved by the optimal fully-connected beamformer \mathbb{W}_{FC}^* and the optimal sub-connected beamformer \mathbb{B}_{SC}^* . The results show that \mathbb{B}_{SC}^* achieves secrecy performance comparable to \mathbb{W}_{FC}^* across a wide SNR range. This observation suggests that the sub-connected scheme can serve as a viable alternative to the fully-connected scheme, offering a favorable trade-off between secrecy performance and implementation complexity. With significantly reduced hardware connectivity at the transmitter, the sub-connected scheme is particularly attractive for practical VLC systems. These results further highlight the potential of sub-connected topologies for the secure VLC system design.

4) *Fully-connected Beamforming Scheme in \mathcal{P}_6* : Simulation parameters follow those used in Sec. VI-B1, with the exception that the algorithm is terminated if any of the following conditions is satisfied:

$$\begin{cases} \|\mathbb{W}^{(k+1)} - \mathbb{W}^{(k)}\|_F \leq 10^{-6}, \\ |f(\mathbb{W}^{(k+1)}) - f(\mathbb{W}^{(k)})| \leq 10^{-6}. \end{cases} \quad (104)$$

Figs. 10 and 11 depict the secrecy rates achieved by the optimal fully-connected beamformer \mathbb{W}_{FC}^* , where an SIMO channel is considered in Fig. 10, and an MIMO channel is considered in Fig. 11. For comparison, the secrecy rates derived in Thm. 2 for the direct-connected scheme are also included. From these figures, it can be observed that the

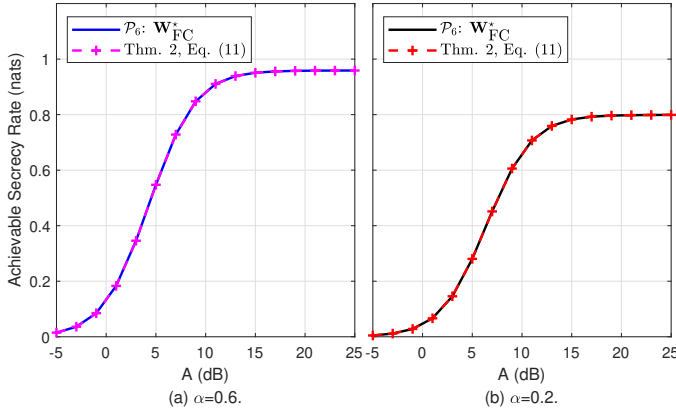


Fig. 10: Achievable secrecy rates of fully-connected beamformer when $\mathbb{H}_B = (\mathbb{H}_B^{1 \times 4})^T$, $\mathbb{H}_E = (\mathbb{H}_E^{1 \times 4})^T$, and $\alpha = \alpha$.

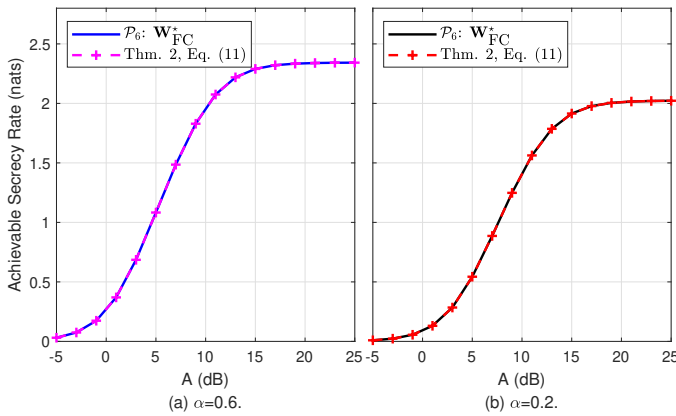


Fig. 11: Achievable secrecy rates of fully-connected beamformer when $\mathbb{H}_B = (\mathbb{H}_B^{2 \times 4})^T$, $\mathbb{H}_E = (\mathbb{H}_E^{2 \times 4})^T$, and $\alpha = \alpha 1_2$.

secrecy performance with beamforming is nearly identical to that achieved without beamforming. This result indicates that under Case II, the deployment of beamformer brings negligible secrecy performance gains. Consequently, beamforming can be safely omitted in this case, leading to a substantial reduction in implementation complexity without sacrificing secrecy performance in practical VLC systems.

VII. CONCLUSION

This paper investigates the secrecy capacity of the MIMO-VLC wiretap channel under both peak- and average-intensity constraints. Two representative quantitative relationships between the transmit and receive apertures are considered: one in which the number of LEDs is larger than or equal to that of the PDs, and another in which it is not. Assuming a truncated exponential input distribution, lower bounds on the secrecy capacity are derived by leveraging the EPI, the GEPI, and the maximum entropy principle. Building upon these theoretical results, beamforming designs are further studied to maximize the achievable secrecy rate for the MIMO-VLC wiretap channels. Although the resulting optimization problem is non-convex, an effective SCA-aided algorithm is developed to obtain efficient solution. Simulation results demonstrate the effectiveness of the proposed beamforming schemes. In

particular, when the number of LEDs is larger than or equal to that of the PDs, the proposed beamformers can significantly improve the secrecy performance of the MIMO-VLC wiretap channel, whereas such performance gains diminish when the number of LEDs is less than that of the PDs.

APPENDIX A PROOF OF LEMMA 3

We first derive the gradient and then the Hessian matrix of $f_B(\mathbb{W})$ in the following [46]. Note that the differential of $f_B(\mathbb{W})$ is

$$\begin{aligned} df_B &= d \left\{ -\frac{n_B}{2} \log \left(1 + |\mathbb{H}_B \mathbb{W}^T \cdot \text{diag}(\mathbf{p}) \cdot \mathbb{W} \mathbb{H}_B^T|^{\frac{1}{n_B}} \right) \right\} \\ &= -\frac{n_B}{2} \frac{1}{1 + |\mathbb{H}_B \mathbb{W}^T \cdot \text{diag}(\mathbf{p}) \cdot \mathbb{W} \mathbb{H}_B^T|^{\frac{1}{n_B}}} \\ &\quad \cdot \frac{1}{n_B} |\mathbb{H}_B \mathbb{W}^T \cdot \text{diag}(\mathbf{p}) \cdot \mathbb{W} \mathbb{H}_B^T|^{\frac{1}{n_B} - 1} \\ &\quad \cdot d |\mathbb{H}_B \mathbb{W}^T \cdot \text{diag}(\mathbf{p}) \cdot \mathbb{W} \mathbb{H}_B^T| \quad (105) \\ &= -\frac{1}{2} \frac{|\mathbb{H}_B \mathbb{W}^T \cdot \text{diag}(\mathbf{p}) \cdot \mathbb{W} \mathbb{H}_B^T|^{\frac{1}{n_B}}}{1 + |\mathbb{H}_B \mathbb{W}^T \cdot \text{diag}(\mathbf{p}) \cdot \mathbb{W} \mathbb{H}_B^T|^{\frac{1}{n_B}}} \text{tr} \left\{ (\mathbb{H}_B \mathbb{W}^T \right. \\ &\quad \cdot \text{diag}(\mathbf{p}) \cdot \mathbb{W} \mathbb{H}_B^T)^{-1} d(\mathbb{H}_B \mathbb{W}^T \cdot \text{diag}(\mathbf{p}) \cdot \mathbb{W} \mathbb{H}_B^T) \left. \right\} \quad (106) \\ &= -\frac{|\mathbb{H}_B \mathbb{W}^T \cdot \text{diag}(\mathbf{p}) \cdot \mathbb{W} \mathbb{H}_B^T|^{\frac{1}{n_B}}}{1 + |\mathbb{H}_B \mathbb{W}^T \cdot \text{diag}(\mathbf{p}) \cdot \mathbb{W} \mathbb{H}_B^T|^{\frac{1}{n_B}}} \text{tr} \left\{ \mathbb{H}_B^T (\mathbb{H}_B \mathbb{W}^T \right. \\ &\quad \cdot \text{diag}(\mathbf{p}) \cdot \mathbb{W} \mathbb{H}_B^T)^{-1} \mathbb{H}_B \mathbb{W}^T \cdot \text{diag}(\mathbf{p}) \cdot d\mathbb{W} \left. \right\}, \quad (107) \end{aligned}$$

where (106) holds since $d|\mathbb{X}| = |\mathbb{X}| \text{tr}(\mathbb{X}^{-1} d\mathbb{X})$, and (107) holds since $\text{tr}\{\mathbb{X}\mathbb{Y}\} = \text{tr}\{\mathbb{Y}^T \mathbb{X}^T\} = \text{tr}\{\mathbb{Y}\mathbb{X}\}$. By (107), we can obtain the gradient of $f_B(\mathbb{W})$ in (70).

For the Hessian matrix of $f_B(\mathbb{W})$, we have

$$\begin{aligned} d^2 f_B &= d \{ df_B \} \\ &\approx -d \left\{ \text{tr} \left\{ \mathbb{H}_B^T (\mathbb{H}_B \mathbb{W}^T \cdot \text{diag}(\mathbf{p}) \cdot \mathbb{W} \mathbb{H}_B^T)^{-1} \mathbb{H}_B \mathbb{W}^T \cdot \text{diag}(\mathbf{p}) \cdot d\mathbb{W} \right\} \right\} \\ &= -\text{tr} \left\{ d \left\{ \mathbb{H}_B^T (\mathbb{H}_B \mathbb{W}^T \cdot \text{diag}(\mathbf{p}) \cdot \mathbb{W} \mathbb{H}_B^T)^{-1} \mathbb{H}_B \mathbb{W}^T \cdot \text{diag}(\mathbf{p}) \cdot d\mathbb{W} \right\} \right\} \\ &= -\text{tr} \left\{ \mathbb{H}_B^T \cdot d(\mathbb{H}_B \mathbb{W}^T \cdot \text{diag}(\mathbf{p}) \cdot \mathbb{W} \mathbb{H}_B^T)^{-1} \mathbb{H}_B \mathbb{W}^T \cdot \text{diag}(\mathbf{p}) \cdot d\mathbb{W} \right\} \\ &\quad - \text{tr} \left\{ \mathbb{H}_B^T (\mathbb{H}_B \mathbb{W}^T \cdot \text{diag}(\mathbf{p}) \cdot \mathbb{W} \mathbb{H}_B^T)^{-1} \mathbb{H}_B (d\mathbb{W}^T) \cdot \text{diag}(\mathbf{p}) \cdot d\mathbb{W} \right\}. \quad (108) \end{aligned}$$

Note that

$$\begin{aligned} &d(\mathbb{H}_B \mathbb{W}^T \cdot \text{diag}(\mathbf{p}) \cdot \mathbb{W} \mathbb{H}_B^T)^{-1} \\ &= -(\mathbb{H}_B \mathbb{W}^T \cdot \text{diag}(\mathbf{p}) \cdot \mathbb{W} \mathbb{H}_B^T)^{-1} d(\mathbb{H}_B \mathbb{W}^T \cdot \text{diag}(\mathbf{p}) \cdot \mathbb{W} \mathbb{H}_B^T) \\ &\quad \cdot (\mathbb{H}_B \mathbb{W}^T \cdot \text{diag}(\mathbf{p}) \cdot \mathbb{W} \mathbb{H}_B^T)^{-1} \\ &= -(\mathbb{H}_B \mathbb{W}^T \cdot \text{diag}(\mathbf{p}) \cdot \mathbb{W} \mathbb{H}_B^T)^{-1} \mathbb{H}_B (d\mathbb{W}^T) \cdot \text{diag}(\mathbf{p}) \cdot \mathbb{W} \mathbb{H}_B^T \\ &\quad \cdot (\mathbb{H}_B \mathbb{W}^T \cdot \text{diag}(\mathbf{p}) \cdot \mathbb{W} \mathbb{H}_B^T)^{-1} - (\mathbb{H}_B \mathbb{W}^T \cdot \text{diag}(\mathbf{p}) \cdot \mathbb{W} \mathbb{H}_B^T)^{-1} \\ &\quad \cdot \mathbb{H}_B \mathbb{W}^T \cdot \text{diag}(\mathbf{p}) \cdot (d\mathbb{W}) \mathbb{H}_B^T (\mathbb{H}_B \mathbb{W}^T \cdot \text{diag}(\mathbf{p}) \cdot \mathbb{W} \mathbb{H}_B^T)^{-1}. \quad (109) \end{aligned}$$

Substituting (109) into (108), we can conclude the Hessian matrix of $f_B(\mathbb{W})$ in (71).

REFERENCES

- [1] L. Zeng et al., "High data rate multiple input multiple output (MIMO) optical wireless communications using white led lighting," *IEEE J. Sel. Areas Commun.*, vol. 27, no. 9, pp. 1654-1662, Dec. 2009.
- [2] H. Kaushal and G. Kaddoum, "Optical communication in space: Challenges and mitigation techniques," *IEEE Commun. Surv. Tutor.*, vol. 19, no. 1, pp. 57-96, Firstquarter 2017.
- [3] N. Chi, Y. Zhou, Y. Wei and F. Hu, "Visible light communication in 6G: advances, challenges, and prospects," *IEEE Veh. Technol. Mag.*, vol. 15, no. 4, pp. 93-102, Dec. 2020.
- [4] Q. H. Spencer, A. L. Swindlehurst and M. Haardt, "Zero-forcing methods for downlink spatial multiplexing in multiuser MIMO channels," *IEEE Trans. Signal Process.*, vol. 52, no. 2, pp. 461-471, Feb. 2004.
- [5] R. Zhang, L. Song, Z. Han and B. Jiao, "Physical layer security for two-way untrusted relaying with friendly jammers," *IEEE Trans. Veh. Technol.*, vol. 61, no. 8, pp. 3693-3704, Oct. 2012.
- [6] Y. Zou, X. Wang and W. Shen, "Optimal relay selection for physical-layer security in cooperative wireless networks," *IEEE J. Sel. Areas Commun.*, vol. 31, no. 10, pp. 2099-2111, Oct. 2013.
- [7] D. W. K. Ng et al., "Robust beamforming for secure communication in systems with wireless information and power transfer," *IEEE Trans. Wireless Commun.*, vol. 13, no. 8, pp. 4599-4615, Aug. 2014.
- [8] Y. Liu et al., "Physical layer security for next generation wireless networks: Theories, technologies, and challenges," *IEEE Commun. Surv. Tutor.*, vol. 19, no. 1, pp. 347-376, Firstquarter 2017.
- [9] H. Peng, Z. Wang, S. Han and Y. Jiang, "Physical layer security for MISO NOMA VLC system under eavesdropper collusion," *IEEE Trans. Veh. Technol.*, vol. 70, no. 6, pp. 6249-6254, Jun. 2021.
- [10] C. Amini, P. Azmi and S. S. Kashaf, "Relay-aided based physical layer security in VLC system with improved noise model," *IEEE Trans. Commun.*, vol. 71, no. 7, pp. 4193-4203, Jul. 2023.
- [11] A. Lapidath, S. M. Moser and M. A. Wigger, "On the capacity of free-space optical intensity channels," *IEEE Trans. Inf. Theory*, vol. 55, no. 10, pp. 4449-4461, Oct. 2009.
- [12] A. Al Hammadi et al., "Non-orthogonal multiple access for hybrid VLC-RF networks with imperfect channel state information," *IEEE Trans. Veh. Technol.*, vol. 70, no. 1, pp. 398-411, Jan. 2021.
- [13] J. -B. Wang, Q. -S. Hu, J. Wang, et al., "Tight bounds on channel capacity for dimmable visible light communications," *J. Light. Technol.*, vol. 31, no. 23, pp. 3771-3779, Dec. 2013.
- [14] A. Mostafa and L. Lampe, "Physical-layer security for MISO visible light communication channels," *IEEE J. Sel. Areas Commun.*, vol. 33, no. 9, pp. 1806-1818, Sept. 2015.
- [15] H. Zaid, Z. Rezk, A. Chaaban, et al., "Improved achievable secrecy rate of visible light communication with cooperative jamming," in *Proc. IEEE Global Conf. Signal Inf. Process. (GLOBASILP)*, Orlando, FL, USA, 2015, pp. 1165-1169.
- [16] M. A. Arfaoui, Z. Rezk, A. Ghrayeb, et al., "On the secrecy capacity of MISO visible light communication channels," in *Proc. IEEE Global Commun. Conf. (GLOBECOM)*, Washington, DC, USA, 2016, pp. 1-7.
- [17] M. A. Arfaoui et al., "Secrecy rate closed-form expressions for the SISO VLC wiretap channel with discrete input signaling," *IEEE Commun. Lett.*, vol. 22, no. 7, pp. 1382-1385, Jul. 2018.
- [18] J. -Y. Wang, C. Liu, J. -B. Wang, et al., "Physical-layer security for indoor visible light communications: Secrecy capacity analysis," *IEEE Trans. Commun.*, vol. 66, no. 12, pp. 6423-6436, Dec. 2018.
- [19] F. M. Al-Sallami et al., "Secrecy capacity and pressure in multiple-lane vehicle-to-vehicle visible light communication channel: An empirical analysis," *IEEE Trans. Veh. Technol.*, vol. 74, no. 9, pp. 13631-13641, Sept. 2025.
- [20] A. Mostafa and L. Lampe, "Optimal and robust beamforming for secure transmission in MISO visible-light communication links," *IEEE Trans. Signal Process.*, vol. 64, no. 24, pp. 6501-6516, Dec. 2016.
- [21] A. Mostafa and L. Lampe, "Physical-layer security for indoor visible light communications," in *Proc. IEEE Int. Conf. Commun. (ICC)*, Sydney, NSW, Australia, 2014, pp. 3342-3347.
- [22] A. Mostafa and L. Lampe, "Securing visible light communications via friendly jamming," in *Proc. IEEE Global Commun. Conf. Workshops (GLOBECOM Wkshps)*, Austin, TX, USA, 2014, pp. 524-529.
- [23] F. Wang et al., "Optical jamming enhances the secrecy performance of the generalized space-shift-keying-aided visible-light downlink," *IEEE Trans. Commun.*, vol. 66, no. 9, pp. 4087-4102, Sept. 2018.
- [24] J. -Y. Wang, H. Ge, M. Lin, et al., "On the secrecy rate of spatial modulation-based indoor visible light communications," *IEEE J. Sel. Areas Commun.*, vol. 37, no. 9, pp. 2087-2101, Sept. 2019.
- [25] M. A. Arfaoui et al., "Physical layer security for visible light communication systems: A survey," *IEEE Commun. Surv. Tutor.*, vol. 22, no. 3, pp. 1887-1908, thirdquarter 2020.
- [26] N. Su et al., "Physical layer security for multi-user MIMO visible light communication systems with generalized space shift keying," *IEEE Trans. Commun.*, vol. 69, no. 4, pp. 2585-2598, Apr. 2021.
- [27] Y. -C. Hsiao, Y. -C. Wu and C. Lin, "Energy-efficient beamforming design for MU-MISO mixed RF/VLC heterogeneous wireless networks," *IEEE Trans. Signal Process.*, vol. 67, no. 14, pp. 3770-3784, Jul. 15, 2019.
- [28] F. Yang, J. Wang and Y. Dong, "Physical-layer security for indoor VLC wiretap systems under multipath reflections," *IEEE Trans. Wireless Commun.*, vol. 21, no. 12, pp. 11179-11192, Dec. 2022.
- [29] K. Wu, Y. Dong, X. Yu, et al., "Relay-aided physical layer security in multi-user VLC with single light source using cooperative jamming," *IEEE Trans. Veh. Technol.*, vol. 74, no. 9, pp. 15002-15007, Sept. 2025.
- [30] H. Le Minh, A. T. Pham, Z. Ghassemlooy, et al., "Secured communications-zone multiple input multiple output visible light communications," in *Proc. IEEE Global Commun. Conf. Workshops (GC Wkshps)*, Austin, TX, USA, 2014, pp. 505-511.
- [31] Z. Chen and H. Haas, "Physical layer security for optical attocell networks," in *Proc. IEEE Int. Conf. Commun. (ICC)*, Paris, France, 2017, pp. 1-6.
- [32] M. A. Arfaoui et al., "On the achievable secrecy rate of the MIMO VLC Gaussian wiretap channel," in *Proc. IEEE Int. Symp. Pers. Indoor Mob. Radio Commun. (PIMRC)*, Montreal, QC, Canada, 2017, pp. 1-5.
- [33] M. A. Arfaoui, A. Ghrayeb, and C. M. Assi, "Secrecy performance of the MIMO VLC wiretap channel with randomly located eavesdropper," *IEEE Trans. Wireless Commun.*, vol. 19, no. 1, pp. 265-278, Jan. 2020.
- [34] A. Chaaban, J.-M. Morvan, and M.-S. Alouini, "Free-space optical communications: Capacity bounds, approximations, and a new sphere-packing perspective," *IEEE Trans. Commun.*, vol. 64, no. 3, pp. 1176-1191, Mar. 2016.
- [35] S. M. Moser, M. Mylonakis, L. Wang, et al., "Asymptotic capacity results for MIMO wireless optical communication," in *Proc. IEEE Int. Symp. Inf. Theory (ISIT)*, Aachen, Germany, 2017, pp. 536-540.
- [36] S. Ma, R. Yang, H. Li, et al., "Achievable rate with closed-form for SISO channel and broadcast channel in visible light communication networks," *J. Light. Technol.*, vol. 35, no. 14, pp. 2778-2787, Jul. 2017.
- [37] L. Li, S. M. Moser, L. Wang and M. Wigger, "On the capacity of MIMO optical wireless channels," *IEEE Trans. Inf. Theory*, vol. 66, no. 9, pp. 5660-5682, Sept. 2020.
- [38] A. Chaaban, Z. Rezk and M. -S. Alouini, "Capacity bounds and high-SNR capacity of MIMO intensity-modulation optical channels," *IEEE Trans. Wireless Commun.*, vol. 17, no. 5, pp. 3003-3017, May 2018.
- [39] I. Csiszár and J. Körner, "Broadcast channels with confidential messages," *IEEE Trans. Inf. Theory*, vol. 24, no. 3, pp. 339-348, May 1978.
- [40] A. E. Gamal and Y.-H. Kim, *Network Information Theory*, Cambridge: Cambridge Univ. Press, 2011.
- [41] R. Zamir and M. Feder, "A generalization of the entropy power inequality with applications," *IEEE Trans. Inf. Theory*, vol. 39, no. 5, pp. 1723-1728, Sept. 1993.
- [42] M. Razaviyayn, "Successive convex approximation: analysis and applications," Diss. University of Minnesota, 2014.
- [43] G. Scutari, F. Facchinei, P. Song, et al., "Decomposition by partial linearization: Parallel optimization of multi-agent systems," *IEEE Trans. Signal Process.*, vol. 62, no. 3, pp. 641-656, Feb. 2014.
- [44] Y. Sun, P. Babu and D. P. Palomar, "Majorization-minimization algorithms in signal processing, communications, and machine learning," *IEEE Trans. Signal Process.*, vol. 65, no. 3, pp. 794-816, Feb. 2017.
- [45] N. J. Higham, "Computing a nearest symmetric positive semi-definite matrix," *Linear Algebra Appl.*, vol. 103, pp. 103-118, 1988.
- [46] X. Zhang, *Matrix analysis and Applications*, Cambridge: Cambridge Univ. Press, 2017.